RESEARCH REPORT

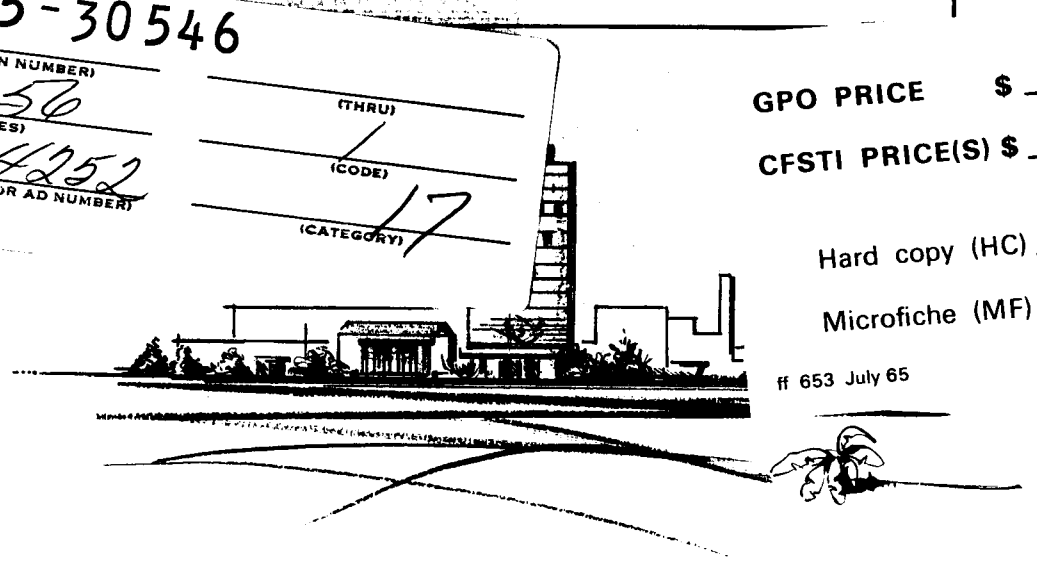

BATTELLE MEMORIAL INSTITUTE

COLUMBUS LABORATORIES

BATTELLE MEMORIAL INSTITUTE

COLUMBUS LABORATORIES • 505 KING AVENUE • COLUMBUS, OHIO 43201

FIELDS OF RESEARCH

Aeronautics — Astronautics
Agricultural Chemistry
Agricultural Economics
Alloy Development
Applied Mathematics
Area Economics
Biochemistry
Biophysics — Bionics
Catalysis — Surface Chemistry
Ceramics
Chemical Engineering
Chemical Processes
Communications Science
Computer Technology
Corrosion Technology
Earth — Atmospheric Sciences
Electrochemistry
Electronics
Energy Conversion
Engineering — Structural Materials
Environmental Systems
Extractive Metallurgy
Extreme-Temperature Technology
Ferrous Metallurgy
Food Technology
Foundry Practice
Fuels — Combustion
Glass Technology
Graphic Arts Technology
Immunology — Cancer Studies
Industrial Economics
Industrial Physics
Information Research
Inorganic Chemistry
Instrumentation
Light Alloys — Rare Metals
Lubricant Technology
Materials Separation — Concentration
Mechanical Engineering
Metal Fabrication Engineering
Metal Finishing
Metallurgical Processes
Microbiology
Microscopy — Mineralogy
Nondestructive Evaluation Technology
Nonferrous Metallurgy
Nucleonics
Ocean Engineering
Organic Chemistry
Organic Coatings
Packaging Research
Particle Dynamics
Petrochemicals
Petroleum Engineering
Pharmaceutical Chemistry
Physical Chemistry
Production Engineering
Psychological Sciences
Pulp — Paper Technology
Radioisotopes — Radiation
Reactor Technology
Refractories
Reliability Engineering
Rubber — Plastics
Semiconductors — Solid-State Devices
Sound — Vibration
Systems Engineering
Textiles — Fibers
Theoretical — Applied Mechanics
Thermodynamics
Transportation
Welding — Metals-Joining Technology
Wood — Forest Products

FINAL SUMMARY REPORT

on

DEVELOPMENT OF IMPROVED THERMOELECTRIC MATERIALS FOR SPACECRAFT APPLICATIONS

to

GEORGE C. MARSHALL
SPACE FLIGHT CENTER
NATIONAL AERONAUTICS AND
SPACE ADMINISTRATION

June 25, 1965

Contract No. NAS8-11452
Control No. DCN 1-4-50-01159-01 & S1 (1F)

For the Period
June 29, 1964, to June 29, 1965

by

E. P. Stambaugh, L. K. Matson, B. G. Koehl,
R. Simon, and E. H. Lougher

BATTELLE MEMORIAL INSTITUTE
505 King Avenue
Columbus, Ohio 43201

Battelle Memorial Institute · COLUMBUS LABORATORIES

505 KING AVENUE COLUMBUS, OHIO 43201 · AREA CODE 614, TELEPHONE 299-3151 · CABLE ADDRESS: BATMIN

June 25, 1965

National Aeronautics and Space Administration
George C. Marshall Space Flight Center
Huntsville, Alabama 35812

Attention PR-EC/Mr. T. Perry

Gentlemen:

Enclosed are 25 copies of the Final Summary Report on your project, "Development of Improved Thermoelectric Materials for Spacecraft Applications" (Contract No. NAS8-11452), covering the period from June 29, 1964, to June 29, 1965.

During this period, significant progress was made toward improvement of the thermoelectric properties of materials in the Ag-Sb-Te and Bi-Sb alloy systems and in development of theoretical criteria for selection and optimization of materials for thermoelectric applications. The results indicate that further efforts along these lines are warranted.

We will be pleased to receive your comments on the report and the conduct of the research.

Very truly yours,

E. H. Lougher
Associate Chief
Physical Chemistry Division

EHL:eh
Enc.

cc: Mr. J. C. Horton
R-P&VE-MEM
National Aeronautics and Space Administration
George C. Marshall Space Flight Center
Huntsville, Alabama 35812

This report was prepared by Battelle Memorial Institute under Contract No. NAS8-11452 for the George C. Marshall Space Flight Center of the National Aeronautics and Space Administration. The work was administered under the technical direction of the Propulsion and Vehicle Engineering Laboratory, Materials Division, of the George C. Marshall Space Flight Center with Mr. Jackson C. Horton acting as project manager.

TABLE OF CONTENTS

DEVELOPMENT OF IMPROVED THERMOELECTRIC MATERIALS FOR SPACECRAFT APPLICATIONS

by

E. P. Stambaugh, L. K. Matson, B. G. Koehl,
R. Simon, and E. H. Lougher

INTRODUCTION

This is the Final Summary Report on the project, "Development of Improved Thermoelectric Materials for Spacecraft Applications", covering the period from June 29, 1964, to June 29, 1965. The program, outlined in PR DCN 1-4-50-01159-01 & S1 and in Battelle's proposal dated June 4, 1964, was carried out under Contract NAS8-11452. The work was a continuation of that conducted by Ohio Semiconductors Division, Tecumseh Products Company, under Contract NAS8-11075.

This research was directed toward the study and optimization of selected materials for use in the thermoelectric cooling in a space environment. The materials studied were Bi-Sb alloys and alloys in the Ag-Sb-Fe-Te-Se system.

ABSTRACT

Experimental effort was directed toward optimization of n- and p-type Bi-Sb alloys for low-temperature thermoelectric cooling and toward the preparation and evaluation of ternary and quaternary alloys in the Ag-Sb-Fe-Se-Te system for use at higher temperatures. Theoretical work was concerned with the development of useful guidelines in the selection and development of improved thermoelectric materials.

Analytical techniques based on $\sigma_o e^r$ and Z(max)T values for screening and evaluating materials for potential thermoelectric applications are discussed. The quantity $\sigma_o e^r$, which can be obtained from the resistivity and Seebeck coefficient values and which is a characteristic constant of a material, is directly indicative of the quality of the electronic transport properties of a single-band material pertinent to its potentialities as a thermoelectric material. It has been established that a $\sigma_o e^r$ of much less than 500 ohm^{-1}-cm^{-1} is a sufficient criterion for rejecting a material without need for further measurements, if the material is known to be essentially extrinsic and to have a single conduction band. If not, the indicated value serves as a rough acceptance guide. If a material has an acceptable $\sigma_o e^r$ value, a good estimate of Z(max)T can be obtained from the Seebeck coefficient, resistivity, and thermal conductivity by plotting the experimental point on a graph of $K/\sigma T$ versus S.

In the Ag-Fe-Sb-Se-Te system, several ternary compositions were studied rather extensively in order to obtain data on single-phase specimens for guidance in development of the more complex alloys. For the Ag-Sb-Se system, it was established that a single-phase region exists in the vicinity of the $AgSbSe_2$ composition and that the better

thermoelectric properties are obtained in those materials having a selenium content in excess of that in the pseudobinary alloy composition (Ag_2Se-Sb_2Se_3). Further work on this ternary system does not appear warranted because of low σ_o values. The highest value of σ_o obtained (85 ohm^{-1}-cm^{-1}) was on a specimen with a nominal composition of $Ag_{25.25}Sb_{24.75}Se_{50}$.

In the Ag-Sb-Te system, single-phase specimens were prepared by zone levelling-zone refining an ingot with a nominal composition of $Ag_{21.3}Sb_{26.8}Te_{51.9}$. Electrical measurements made on these single-phase specimens revealed that both the Seebeck coefficient and Hall coefficient were positive, in contrast to a positive Seebeck coefficient and negative Hall coefficient obtained on specimens containing trace amounts of a minor phase. The composition of a single-phase region was found by wet-chemical analysis to be $Ag_{20.7}Sb_{27.5}Te_{51.8}$. From the σ_o values obtained to date on selected specimens (500 and 800 ohm^{-1}-cm^{-1} at 300° and 400°K, respectively) this system shows promise for thermoelectric cooling applications and, therefore, warrants further study.

In study of the Ag-Sb-Te-Se alloys, it was observed that the most nearly single-phase specimen (nominal composition of $Ag_{20}Sb_{28}Te_{26}Se_{26}$) had the highest σ_o. Additional work will need to be conducted on this alloy system to ascertain its potentiality for thermoelectric cooling applications.

Specimens of composition $AgFeSe_2$ and $AgFeTe_2$ were polyphase and showed no promise as thermoelectric materials.

Of the four undoped (n-type) Bi-Sb alloys studied (5, 8, 12, and 14 atomic percent antimony), the $Bi_{92}Sb_8$ alloy had the highest value of S^2/ρ over most of the temperature range of interest. Light doping of the $Bi_{86}Sb_{14}$ alloy with tin, a p-type doping agent, increased the n-type S^2/ρ value in the vicinity of 300°K above that of the undoped alloy. The Seebeck-coefficient values of tellurium-doped alloys (n-type) were very low, indicating that the carrier concentration was too high. All p-type specimens prepared had low S^2/ρ values; it appears improbable that p-type Bi-Sb alloys will be useful for thermoelectric-cooling applications. The anisotropy of the Seebeck coefficient and resistivity in the Bi-Sb alloys was found to be dependent on the degree of doping.

From the results attained on Bi-Sb alloys during this contract period, it is evident that further research on the system is warranted.

The general theory of the thermoelectric figure of merit for materials characterized by a multiplicity of parabolic electron-energy bands was applied to determine the relationship between Z(max)T, the maximum dimensionless figure of merit as optimized with respect to impurity doping, and the basic material parameters of the single-band, two-band, and three-band models over wide ranges of values of these parameters. This permitted the ranges of validity of the one- and two-band models to be more clearly delineated.

The general qualitative features of the thermoelectric behavior of materials were found to be adequately accounted for on the basis of an equivalent two-band model under many circumstances of interest. The three-band and higher-band-multiplicity models are required mainly to account for certain details of behavior and to obtain better accuracy where needed. It is shown how the two-band model may be used to obtain the value of $(ZT)_{max}$ for materials, the dimensionless figure of merit as optimized with respect to both impurity doping and temperature. This latter quantity is the one of major

interest in rating potential thermoelectric materials. Optimization with respect to alloy composition can also be made if the variations of the basic material parameters of the two-band model with alloy composition can be estimated.

The delineations of the basic material parameters of the one-, two-, and three-band models in terms of the various material constants and of their effects on the value of Z(max)T and $(ZT)_{max}$ enable a critical examination to be made of proposed criteria for material selection. In particular, it was found that any criteria based on assumed advantages of particular crystal symmetries or degrees of anisotropy have no substantial basis in theory or in fact. Higher values of the electronic portion of the single-band material parameter, σ_o, would be expected to be obtained for band structures consisting of a multiplicity of equivalent extrema with a high degree of effective-mass anisotropy in the neighborhood of each extremum. However, this desirable condition is not necessarily directly correlatable with any overall crystal anisotropy or any particular crystal structure. Likewise, material-selection criteria based on a minimum degree of ionicity in the chemical bond were found to be of little value. Examination of the various material parameters of the single-band and two-band models showed that some medium degree of ionicity in the chemical bond should have a beneficial effect on the value of Z(max)T.

The values of the equivalent two-band-model parameters were computed and tabulated for the common elemental and binary-compound semiconductors and semimetals on the basis of data available in the literature. Preliminary observations made from these tabulations seem to confirm the above conclusions regarding the validities of proposed selection criteria. These tabulations should aid in the search for improved material-selection criteria.

DETAILS AND DISCUSSION

Experimental and theoretical studies have been conducted with the objective of development of improved thermoelectric materials for spacecraft applications. Experimental work was concerned with evaluating the Ag-Sb-Fe-Se-Te and Bi-Sb alloy systems. The theoretical effort was concerned with (1) correlation of chemical considerations with the theory, developed previously at Battelle and elsewhere, of the interrelation of fundamental semiconductor characteristics (band gap, degree of doping, symmetry of band structure, etc.) with thermoelectric performance parameters, and (2) the development of useful guidelines in the selection and development of improved thermoelectric materials.

Experimental Investigation

Material-Evaluation Criteria

In previous theoretical studies at Battelle, analytical techniques[1,2]* have been developed for the evaluation and screening of materials for potential thermoelectric applications. Screening of materials is based on the quantity $\sigma_o e^r$ whereas evaluation is based on the value of $Z_{(max)}T$.

*References are listed at end of report.

As shown in the theoretical section of this report, the quantity $\sigma_o e^r$ is a valid measure of the quality of the charge-carrier-transport contribution to the thermoelectric figure of merit. The value of $\sigma_o e^r$ can be readily determined for extrinsic materials from the resistivity and Seebeck-coefficient values, using the procedure outlined in the First Quarterly Progress Report. Consequently, it has been used previously at Battelle as a convenient criterion for the rapid screening of materials. Materials that are adjudged to be acceptable under the $\sigma_o e^r$ criterion are candidates for further testing to ascertain their thermoelectric potentialities.

The value of $\sigma_o e^r$ used as a dividing line between qualified acceptance and rejection of materials is somewhat arbitrary. The better thermoelectric materials seem to have $\sigma_o e^r$ values in the neighborhood of 10^3 ohm^{-1}-cm^{-1}. The room-temperature values of $\sigma_o e^r$ for n-Bi_2Te_3 and p-Bi_2Te_3 are 1600 and 1200 ohm^{-1}-cm^{-1}, respectively.(3) The room-temperature $\sigma_o e^r$ of $(Bi_2Te_3)_{90}(Bi_2Se_3)_{10}$ alloy is 1400 ohm^{-1}-cm^{-1}. The n-$Ge_{70}Si_{30}$ alloy has a room-temperature $\sigma_o e^r$ value of 1200 ohm^{-1}-cm^{-1}. Fortunately, from the viewpoint of selecting materials for $(ZT)_{max}$ as well as for Z(max)T at a given temperature, the value of $\sigma_o e^r$ is not too temperature sensitive (σ_o would be independent of temperature if m_d were temperature independent and μ varied strictly as $T^{-3/2}$). The values of $\sigma_o e^r$ of n-Bi_2Te_3 and p-Bi_2Te_3 at T = 150°K are about 1500 and 1400 ohm^{-1}-cm^{-1}, respectively. $\sigma_o e^r$ of n-$Ge_{30}Si_{70}$ at 1100°K is 1400 ohm^{-1}-cm^{-1}.

In order to ensure that no material of potential thermoelectric importance would be inadvertently missed in a material survey, the threshold value of $\sigma_o e^r$ for further evaluation has been set at about 500 ohm^{-1}-cm^{-1}. A material with a σ_o value of 500 ohm^{-1}-cm^{-1} would have to have a K_L value of about 0.005 watt/cm°C in order to begin to be of thermoelectric interest (β = 0.22 at room temperature). The value of 500 ohm^{-1}-cm^{-1} for $\sigma_o e^r$ is based on the material's being extrinsic and having single-band conduction. If the material is not known to be single-band and extrinsic, the indicated $\sigma_o e^r$ values serve as a rough acceptance criterion for further consideration rather than as a good rejection criterion.

If further consideration is indicated from the $\sigma_o e^r$ values, then a good estimate of the maximum figure of merit of the material, Z(max)T, with respect to impurity doping can be obtained from the Seebeck coefficient (S), resistivity (ρ), and thermal conductivity (K) values on a single specimen. This is done by plotting the experimental point $(S, K\rho/T)$ on a graph of $K/\sigma T$ versus S [see Reference (1)]. The position of the point on this characteristic curve also indicates whether the measured specimen is underdoped, overdoped, or about optimally doped. This analysis is for materials with single-band conduction. However, it has been extended to include the two-band (electrons and holes) case.(2) As the impurity doping is changed, it is observed that a plot of S versus $K\rho/T$ is a closed-loop curve with two maxima of $ZT = S^2/(K\rho/T)$ along this curve, one for negative Seebeck coefficient and one for positive Seebeck coefficient. Thus, measured values of S and $K\rho/T$ for only a few differently doped specimens are, in principle, sufficient to outline the characteristic curve for a given material, and hence, to determine the values of the pertinent dimensionless parameters and also the two values of Z(max)T.

Effects of Inhomogeneities

In evaluating a system for possible thermoelectric applications, it is important to conduct the electrical measurements on specimens that are homogeneous and single

phase. Attainment of single-crystal specimens is desirable, of course, but this requirement is not nearly so important as that of homogeneity and single-phase composition, since electrical measurements conducted on inhomogeneous, polyphase specimens can be misleading. As a matter of fact, it is impossible to determine with confidence the potentiality of a system for thermoelectric-cooling applications from data collected from inhomogeneous materials.

A high degree of inhomogeneity in a material leads to a lower figure-of-merit value than if the material is homogeneous.[4, 5] The lower figure of merit for an inhomogeneous material results from an increase in the thermal conductivity and a decrease in the Seebeck coefficient by the circulating-current effect, as discussed below.

Consider an idealized inhomogeneous specimen consisting of Regions 1 and 2 of different composition, as illustrated in Figure 1. If a temperature gradient is imposed across the specimen as shown, circulating currents (indicated by arrows) will be set up as a result of the difference in Seebeck coefficient between the two regions. As the currents cross the boundaries between the two regions at the high-temperature end ($T+\Delta T$), heat is absorbed by the Peltier effect. As they cross the boundaries at the low-temperature end (T), heat is evolved by the Peltier effect. This effect increases the effective thermal conductivity of the material. Such behavior has been observed in Bi_2Te_3-Bi_2Se_3 alloys[6], $BiSbTe_3$[7], $AgSbTe_2$[8], etc. In each semiconductor compound or alloy, the more homogeneous specimens exhibited the best thermoelectric properties.

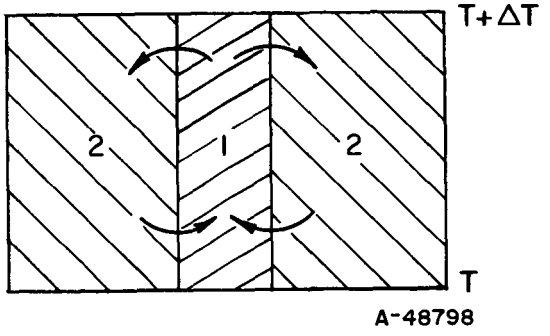

FIGURE 1. CIRCULATING CURRENTS RESULTING FROM INHOMOGENEITIES

Other transport properties also are sensitive to inhomogeneities in materials. Thus, in determining the transport properties of any system, the importance of the homogeneity of the specimens can be an overriding factor. Therefore, throughout this investigation, effort was directed toward the preparation and evaluation of single-phase specimens of compounds and alloys.

Ternary Compounds

This part of the program was concerned with the evaluation of Ag-Sb-Te alloys and more complex materials derived by partial substitution of Fe and Se in the Ag-Sb-Te alloy lattice. For guidance in the development of these complex materials, data were

needed on the properties of single-phase specimens of ternary compounds in the Ag-Fe-Sb-Se-Te system.

Preparation. Four methods were used in preparation of specimens of Ag-Sb-Te, Ag-Sb-Se, Ag-Fe-Te, and Ag-Fe-Se alloys. These were (1) furnace cool-anneal, (2) quench-anneal, (3) Bridgman, and (4) a combination of zone levelling and zone refining. These methods have been used extensively at Battelle to prepare single-phase, homogeneous specimens of semiconducting compounds and alloys. The methods are discussed in the First and Third Quarterly Progress Reports.

Evaluation. Preliminary evaluation of each ingot was made by metallographic examination of polished and etched surfaces and by measurement of approximate values of Seebeck coefficient (S) and resistivity (ρ) at various points along the ingot by thermoelectric hot-probe and four-probe resistivity measurements*. More detailed measurements were made on specimens that had interesting properties and adequate homogeneity.

Ag-Sb-Se System. Single-phase Ag-Sb-Se ingots were prepared by the furnace cool-anneal method under the conditions shown in the Second Quarterly Progress Report. Electrical properties and degree of homogeneity as functions of composition are listed in Table 1.

It was determined that a single-phase region in this system extends from at least $Ag_{24.5}Sb_{25.5}Se_{50}$ to $Ag_{25.4}Sb_{24.6}Se_{50}$. Since only a small portion of the phase diagram has been examined, this region may be larger than noted and there may be other single-phase regions.

As seen in Table 1, those specimens having a selenium content in excess of that of a pseudobinary composition (E > 0) had the higher values of σ_o. In general, the values are low, although some improvement was attained by varying the composition from the $Ag_{25}Sb_{25}Se_{50}$ composition. The highest σ_o (85 ohm^{-1}-cm^{-1}) was obtained on a specimen of nominal composition $Ag_{1.01}Sb_{0.99}Se_2$ ($Ag_{25.25}Sb_{24.75}Se_{50}$; E = +0.25). It appears that alloys with composition in the neighborhood of $AgSbSe_2$ have little promise for use in thermoelectric cooling.

Ag-Sb-Te System. Study of Ag-Sb-Te alloys was concerned with the effects of composition and method of preparation on the homogeneity and thermoelectric properties. As with Ag-Sb-Se alloys, the methods of preparation used were: quench-anneal, furnace cool-anneal, Bridgman, and zone levelling-zone refining. Preparative conditions for the ingots are shown in the Second and Third Quarterly Progress Reports; composition and electrical data are shown in Table 2.

*These are rapid techniques for obtaining approximate values of Seebeck coefficient and resistivity at several points on a specimen. The hot-probe method is based upon the deflection of a calibrated galvanometer connected between two probes – one heated, the other at room temperature – placed in contact with the specimen. The sign and magnitude of the deflection indicate the conductivity type and the approximate value of the Seebeck coefficient. The four-probe technique employs four closely spaced point probes in a row, which are placed in contact with the specimen. Current is passed between the two end probes, and the potential drop between the inner pair is measured. The resistivity can be calculated from the values of the current and potential drop and the probe spacing.

TABLE 1. COMPOSITION AND ELECTRICAL DATA ON $Ag_xSb_ySe_w$ ALLOYS

Ingot	Nominal Composition, atomic percent			Composition Variables		Approximate Percentage of Second Phase(c)	Resistivity, (d) ohm-cm	Seebeck Coefficient, (d) $\mu V/°K$	σ_o, (d) $ohm^{-1} - cm^{-1}$
	Ag, x	Sb, y	Se, z	E(a)	A(b)				
21561-3	25.0	25.0	50.0	0	0	0	4.4 to 4.7	+50 to +500 (mostly +300 to +400)	2
-85	23.7	25.8	50.5	-0.05	+2.1	0	$>10^3$	+50	$<10^{-2}$
-59	25.25	24.75	50.0	+0.25	-0.05	0	1.4 to 1.7 x 10^{-2}	+180 to +220	85
-97	25.5	25.0	49.5	-0.75	-0.5	1.5	0.1 to $>10^{-3}$	-20 to +125	0.7
-96	25.0	24.5	50.5	+1.25	+0.5	2	1.4 to 2.1 x 10^{-2}	+70 to +170	30
-84	24.3	24.3	51.4	+2.8	0	2.5	2.4 x 10^{-2}	+200	55
-83	26.0	24.0	50.0	+1	-2	4.5	1.25 x 10^{-2}	+170	75
22086-11	25.6	24.4	50.0	+0.6	-1.2	1.5	2 x 10^{-2}	+110 to +140	30
-12	24.5	25.0	50.5	+0.75	-0.5	2	3.3 x 10^{-2}	+80 to +110	11
-13	24.5	25.5	50.0	-0.5	+1.0	0	0.5	+40 to +70	0.4

(a) $E = w - \frac{x}{2} - \frac{3y}{2}$ = atomic percentage of selenium in excess of the percentage in a pseudobinary alloy of Ag_2Se and Sb_2Se_3.

(b) $A = y - x$ = atomic percentage by which antimony exceeds silver in the alloy.

(c) Based on the percent of area of second phase in polished sample. Chemical etch did not reveal any other phases.

(d) Approximate values obtained by four-probe and hot-probe methods.

TABLE 2. COMPOSITION AND APPROXIMATE-ROOM TEMPERATURE ELECTRICAL DATA ON $Ag_xSb_yTe_z$ ALLOYS

Sample	Ingot	Method of Preparation[a]	Distance From End First to Freeze, inches	Composition atomic percent[b] Ag, x	Sb, y	Te, z	Composition Variables E[c]	A[d]	Concentration of Minor Phases, percent[e] Polished	Etched	Resistivity, ρ, ohm-cm[f]	Seebeck Coefficient, S, $\mu V/°K$[f]	σ_o, $ohm^{-1}-cm^{-1}$[f]
1	21561-16	ZL-ZR	0.3	20	27.9	52.1	0.25	7.9	<1	<1	4.2×10^{-3}[g]	+213[g]	370[g]
2	21561-16	"	0.5	--	--	--	0.5[g]	7.2[g]	--	--	3.9×10^{-3}	+215	420
3	21561-16	"	1.0	--	--	--	1.05[g]	5.7[g]	--	--	3.4×10^{-3}	+220	510
4	21561-16	"	1.1	21.3	26.8	51.9	1.05	5.5	<1	<1	3.3×10^{-3}[g]	+220[g]	520[g]
5	21561-16	"	2.0	--	--	--	0.5[g]	4.0[g]	--	--	3.8×10^{-3}	+225	490
5'	21561-16	"	1.7	--	--	--	--	--	--	--	3.5×10^{-3}[h]	+215[h]	520[h]
6	21561-16	"	2.5	22.8	26.3	50.9	0.05	3.5	<1	<1	4.8×10^{-3}[g]	+230[g]	410[g]
7	21561-16	"	3.0	--	--	--	-0.4[g]	3.1[g]	--	--	5.7×10^{-3}[h]	+245[h]	430[h]
8	21561-1	FC-A	--	25	25	50	0	0	~5	0	0.97×10^{-2}[h]	+225[h]	200[h]
9	21561-16	ZL-ZR	7.3	>25	<25	<50	--	--	~15	0	1.3×10^{-2}	+75[h]	25[h]
10	21561-64	Q-A	--	24	29	47	-8.5	5	~80	--	--	--	--
11	21561-63	"	--	22	27	51	-0.5	5	~30	--	--	--	--
12	21561-79	"	--	21.6	26.7	51.7	0.85	5	~1	--	5.1×10^{-3}	+135	130
13	21561-80	"	--	21.3	26.3	52.4	2.3	5	~4	--	1.9×10^{-3}	+82	160
14	21561-81	"	--	20.9	25.9	53.2	3.9	5	~10	--	--	--	--
15	21561-62	"	--	20	25	55	7.5	5	~20	--	--	--	--
16	21561-95	"	--	19	28.6	52.4	0	+9.6	0	5	1.3 to 2.2×10^{-2}	+245 to +270	150
17	21561-92	ZL-ZR	0.5	--	--	--	--	--	0	>1	3.5×10^{-3}	+195	365
18	21561-92	"	0.8	18.0	29.0	53.0	--	--	--	--	--	--	--
18'	21561-92	"	0.9	18.0	29.0	53.0	--	--	0	0	2.72×10^{-3}[h]	+140[h]	260[h]
19	21561-92	"	1.0	--	--	--	--	--	--	--	3.0×10^{-3}	+195	425
20	21561-92	"	2.1	--	--	--	--	--	0.03	0	2.5×10^{-3}	+130	230
21	21561-92	"	3.0	20.7	27.5	51.8	--	--	--	--	2.9×10^{-3}	+195	440
22	21561-92	"	3.9	--	--	--	--	--	0.9	0	2.8×10^{-3}	+195	455
23	21561-92	"	5.0	--	--	--	--	--	--	--	1.9×10^{-3}	+80	160
24	21561-92	"	5.7	--	--	--	--	--	3.3	0	2.0×10^{-3}	+90	170
25	21561-92	"	6.5	--	--	--	--	--	--	--	2.8×10^{-3}	+100	140
26	21561-92	"	7.5	--	--	--	--	--	11.5	0	3.8×10^{-3}	+100	105
27	22086-14	B-Q	--	21.3	26.8	51.9	+1.05	+5.5	2	>10	4×10^{-3}	+80 to +180	~150
28	22086-15	B-FC	--	21.3	26.8	51.9	+1.05	+5.5	1	0	5×10^{-3}	+210	~300
29	22086-21	Q-A	--	19	29.6	51.4	-2.7	+10.6	0	>20	1.4×10^{-2}	+190	85
30	22086-22	Q-A	--	19	27.6	53.4	+2.5	+8.6	6	Dendritic	8×10^{-4}	+50	230

(a) Q = quenched; A = annealed; B = Bridgman; FC = furnace cooled; ZL = zone levelled; ZR = zone refined.

(b) All nominal compositions except Samples (1), (4), (6), (18), and (22), which are by chemical analysis. Nominal compositions of Ingots 21561-16 and 21561-92 from which samples listed were removed were $Ag_{25}Sb_{25}Te_{50}$ and $Ag_{21.3}Sb_{26.8}Te_{51.9}$, respectively.

(c) E = z-x/2-3y/2 = atomic percentage of tellurium in excess of that in a pseudobinary alloy of Ag_2Te and Sb_2Te_3.

(d) A = y-x = atomic percentage by which antimony exceeds silver in the alloy.

(e) Approximate concentration as detected on surface prepared as noted.

(f) Approximate values obtained by four-probe and hot-probe methods, except where otherwise noted.

(g) Extrapolated or interpolated value.

(h) Data from detailed measurements as functions of temperature (see Figures 2, 3, and 4).

Microscopic examination of polished and etched surfaces* revealed that single-phase materials were prepared only by the zone levelling-zone refining method. Those prepared by the other methods contained two minor phases – one phase revealed by polishing the surface, the other by etching. The minor phase on the polished surface had the appearance of a cellular-like structure (Figure 1g, Second Quarterly Progress Report) with the minor phase making up the cell walls. The other minor phase, brought out by chemical etching, was scattered throughout the specimens. This phase has been identified as a Widmanstätten precipitate of Sb_2Te_3 on the (111) planes of the fcc structure[9].

In the specimens prepared by all methods other than zone levelling-zone refining, the two minor phases were intermingled. However, by zone refining it was possible to separate these phases and prepare single-phase materials. The phase revealed by polishing was concentrated in the end of the ingot last to freeze, whereas that revealed by etching was concentrated in the end first to freeze. In an intermediate region, the material appeared to be single phase. Although the extent of this single-phase region has not been determined, it has been established that it includes the composition $Ag_{20.7}Sb_{27.5}Te_{51.8}$ (Ingot 21561-92, Sample 22 in Table 2).

In general, specimens from the zone levelled-zone refined ingots (the more nearly single-phase specimens) had much higher values of σ_o than did specimens from ingots prepared by other methods (two minor phases present). The effects of inhomogeneity on the thermoelectric properties of selected specimens were further evidenced in a series of electrical measurements as functions of temperature. As seen in Figures 2, 3, and 4, a highly polyphase specimen (Specimen 9) had the lowest Seebeck coefficient (p-type), the highest resistivity, and the largest Hall coefficient (n-type). Specimens which were more nearly single phase had larger (positive) Seebeck-coefficient values, lower resistivities, and smaller (negative) Hall-coefficient values (Sample 5'). (The negative Hall coefficient is believed to be associated with the presence of the minor phases[5].) Seebeck-coefficient and Hall-coefficient values of a single-phase specimen (Sample 21, Table 2) were both positive. This specimen (composition by chemical analysis = $Ag_{20.7}Sb_{27.5}Te_{51.8}$) was prepared by zone levelling-zone refining an ingot with a nominal composition of $Ag_{21.3}Sb_{26.8}Te_{51.9}$ (Ingot 21561-92).

From the results obtained, the Ag-Sb-Te system shows promise for thermoelectric-cooling applications over a wide temperature range. The thermal conductivity is low, and σ_o values exhibit an increasing trend with temperature over the range in which measurements have been made. σ_o values greater than 500 ohm^{-1}-cm^{-1} and 750 ohm^{-1}-cm^{-1} have been obtained at 300° and 400°K, respectively (Specimen 5').

$AgFeSe_2$ and $AgFeTe_2$ Systems. All $AgFeTe_2$ and $AgFeSe_2$ ingots prepared were polyphase (Second Quarterly Progress Report). Those prepared by furnace cool-anneal and quench-anneal contained two phases of approximately equal concentration, as well as a minor third phase. In ingots prepared by zone levelling-zone refining, one major phase predominated at one end of the ingot and the second predominated at the other. The first half of a $AgFeTe_2$ ingot (21561-37) also contained a trace (less than 5 percent) of a third phase. Chemical analysis of a specimen from near the tail (last to freeze) end of this ingot showed the composition to be $Ag_{4.7}FeTe_{4.3}$. This can be rewritten in the form $(Ag_{4.7}Te_{2.3})(FeTe_2)$ or, approximately, $(2.3Ag_2Te)(FeTe_2)$, suggesting that the phases present may have been predominantly Ag_2Te and $FeTe_2$. The melting point of the

*Thirty-second etch in $45H_2O$:$55HNO_3$ followed by rinse in deionized water.

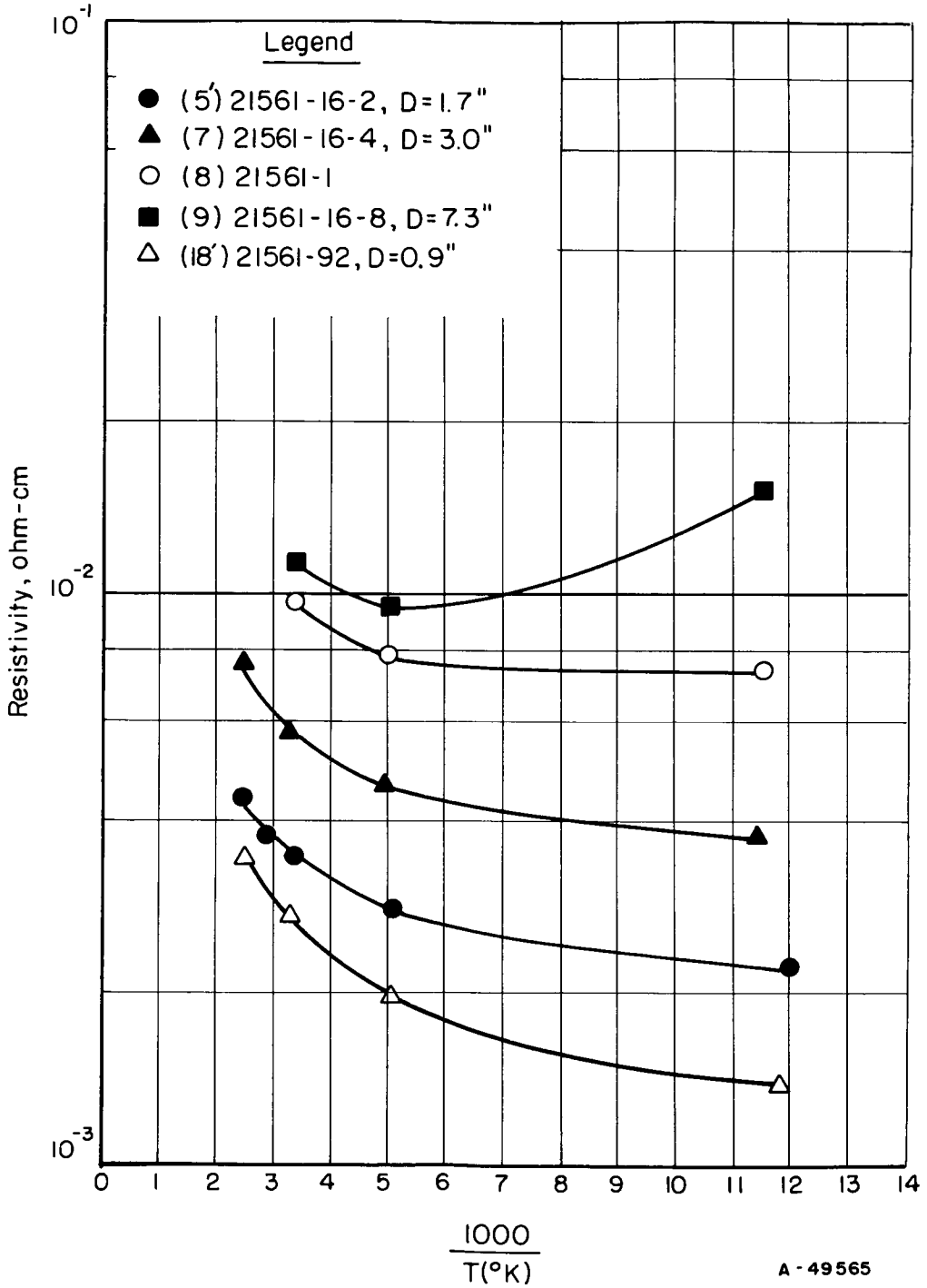

FIGURE 2. RESISTIVITY VERSUS RECIPROCAL TEMPERATURE FOR $Ag_xSb_yTe_z$ ALLOYS

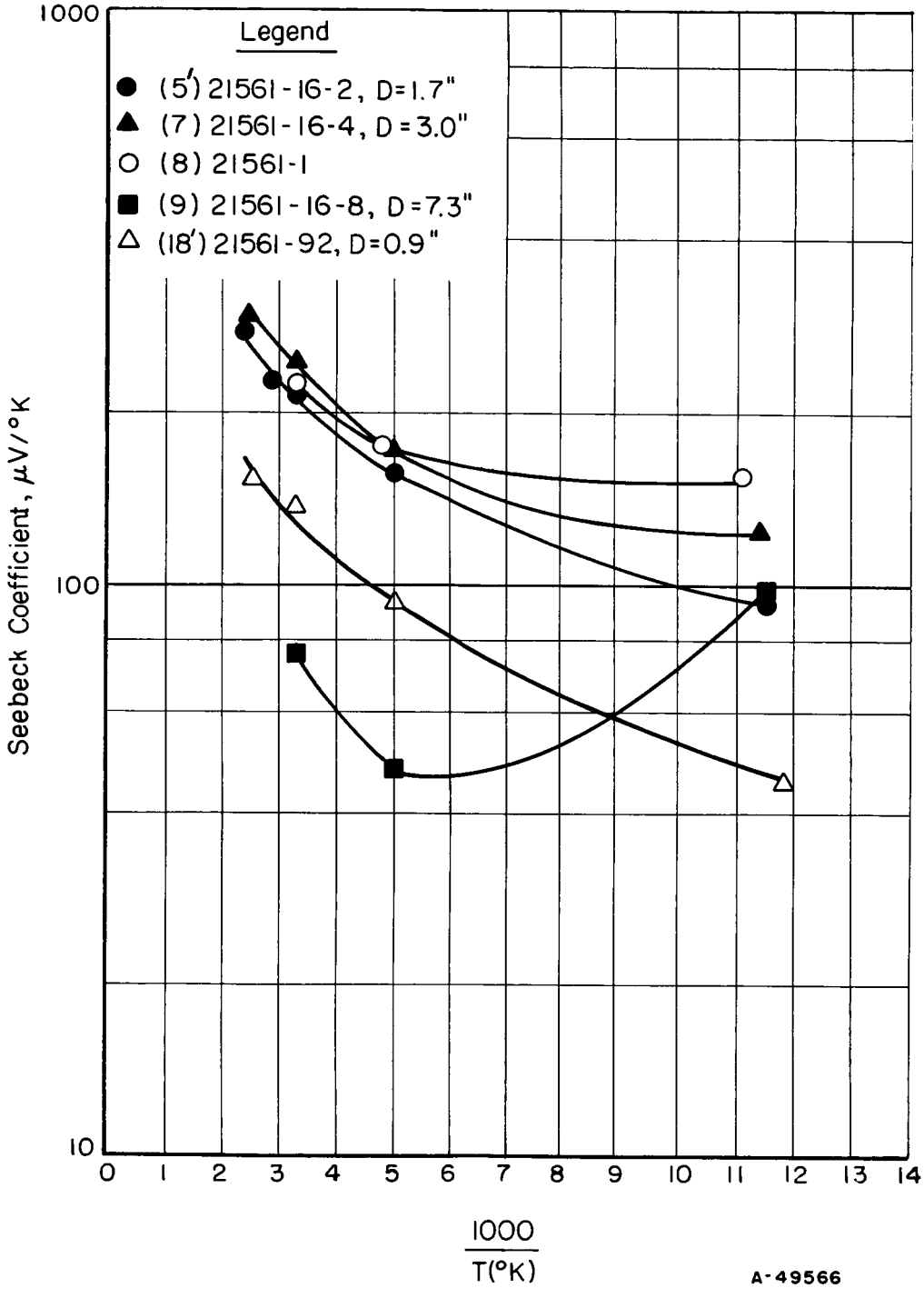

FIGURE 3. SEEBECK COEFFICIENT VERSUS RECIPROCAL TEMPERATURE FOR $Ag_xSb_yTe_z$ ALLOYS

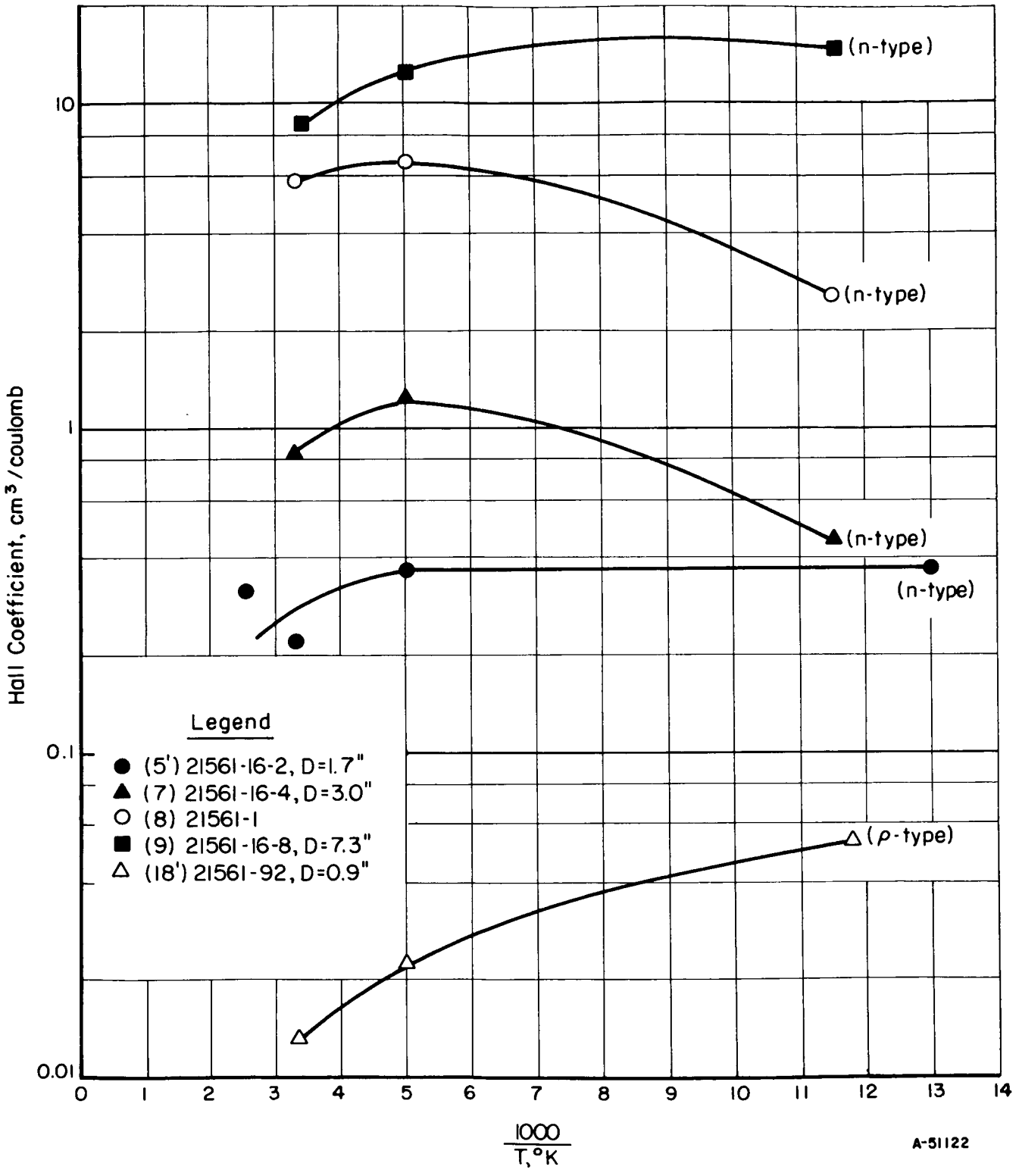

FIGURE 4. HALL COEFFICIENT AT 8000 GAUSS VERSUS RECIPROCAL TEMPERATURE FOR $Ag_xSb_yTe_z$ ALLOYS

specimen, as determined by thermal analysis, was lower than those of the above binary compounds, but the difference could conceivably be due to eutectic formation. It appears doubtful if ternary compounds exist in these two systems.

σ_o values from four-probe and hot-probe data were low (<150 ohm^{-1}-cm^{-1}). In view of these low values and the polyphase character of the ingots, further work on these systems for thermoelectric-cooling applications does not appear warranted.

Quaternary System

Ag-Sb-Se-Te Alloys. Several ingots in the Ag-Sb-Se-Te quaternary system, as listed in Table 3, were made. These compositions may be considered as pseudobinary alloys obtained by mixing $Ag_{21.3}Sb_{26.8}Te_{51.9}$ and $Ag_{25.25}Sb_{24.75}Se_{50}$ in varying proportions. These two ternary compositions were chosen because they had been prepared as single-phase or nearly single-phase materials and had about the best thermoelectric properties measured thus far in each system. The alloys were prepared by the furnace cool-anneal method.

TABLE 3. COMPOSITION OF $Ag_xSb_yTe_zSe_w$ ALLOYS

Ingot	Nominal Composition, atomic percent			
	Ag	Sb	Te	Se
21561-93	23.28	25.78	25.95	25.0
22086-16	22.3	26.3	38.9	12.5
-19	25.0	25.0	25.0	25.0
-20	20.0	28.0	26.0	26.0

Preliminary examination of polished specimens revealed no minor phases in Ingot 22086-20 and only about 1 to 3 percent of a minor phase in the other ingots. However, examination of chemically etched specimens (55 percent HNO_3 for 30 seconds) revealed that all were polyphase. A specimen from Ingot 22086-20 contained about 5 percent of a phase similar to that seen in polished, unetched specimens of quenched $AgSbTe_2$. A specimen from Ingot 22086-19 contained about 10 percent of a similar phase. A specimen from Ingot 22086-16 was polyphase and dendritic.

σ_o values based on four-probe and hot-probe data were low – ranging from 3 to 75 ohm^{-1}-cm^{-1}, with the most nearly single-phase specimen (22086-20) having the highest σ_o value. The low values may result, at least partially, from the polyphase character of the specimens.

Further study of this system will be required in order to evaluate it for thermoelectric-cooling applications.

Bismuth-Antimony Alloys

A study was conducted on the optimization of Bi-Sb alloys for low-temperature thermoelectric-cooling applications. Emphasis was placed on (1) preparation of n- and p-type alloys, and (2) measuring Seebeck-coefficient and resistivity values on single-crystal specimens as functions of temperature and crystal orientation.

Initial (and most extensive) study was made on the alloys containing approximately 14 percent antimony. This composition was chosen because it has been reported that it has about the maximum energy gap (0.024 ev) in the Bi-Sb alloy system[10]. All other variables being equal, the alloy with the largest band gap would have the highest figure of merit, since the contribution of ambipolar diffusion to the thermal conductivity as well as partial cancellation of the Seebeck coefficient by minority carriers would be minimized.

Preparation. The alloy specimens listed in Table 4 were studied. They were prepared by zone levelling at a crystallization rate of 3.2 cm per hour, using rf induction heating and coupling directly to the melt. A quartz boat of semicircular cross section, coated with carbon* to reduce stray nucleation at the melt-container interface, was used as the container.

TABLE 4. COMPOSITION OF BISMUTH-ANTIMONY ALLOYS

Ingot	Nominal Composition[a], atomic percent			
	Bi	Sb	Sn	Te
21590-1	86	14	--	--
-5	82.8	13.8	3.4	--
-15	88	12	--	--
-16[b]	95	5	--	--
-18	84.2	14.0	--	1.8
-27	84.1	14.0	1.9	--
-31	84.9	14.2	--	0.9
-45	85.5	14.3	--	0.2
-47	85.5	14.2	0.2	--
-49	85.6	14.3	0.08	--
-56	85.6	14.3	--	0.073
-58	84.9	14.1	1.0	--
-61	88	12	(0.08 mol % CuBr)	
-62	85.68	14.28	--	0.037
-64	92.0	8.0	--	--
-67	86.3	11.7	2.0	--
-68	87.21	11.78	0.95	--
-69	88.06	11.90	--	0.038
-73	85.68	14.28	0.04	--

(a) All compositions given in the discussion of Bi-Sb alloys are nominal, with the exception of that for Specimen 21590-1 (undoped $B_{85.4}Sb_{14.6}$) which was determined by chemical analysis.

(b) This ingot was prepared previously on another project.

*Carbon-coated quartz boats were prepared by pyrolysis of acetone at ≈750°C in an argon atmosphere.

The preparation procedure was as outlined in the First Quarterly Progress Report. Each ingot, weighing approximately 375 g and measuring about 25 cm by 2.2 cm, was given from 6 to 30 zone-levelling passes. The orientation of the principal cleavage plane (plane perpendicular to the c-axis) was controlled by seeding, in order to obtain specimens with the desired dimensions (16-20 mm by 4-5 by 4-5 mm) for electrical measurements. Without seeding, the cleavage plane was generally oriented at 45°-60° with respect to the longitudinal axis of the ingot and rotated about the vertical axis.

The preferred direction of growth at this crystallization rate appears to be with the cleavage plane approximately vertical and at an angle of about 75° with respect to the longitudinal axis. Ingots grown with this orientation are shown in Figure 5 (b and c), Second Quarterly Progress Report. By using seeds with this orientation, the cleavage plane rarely shifted. Ingots with other orientations were grown, but shifting of the cleavage plane was a problem.

Electrical Measurements. The Seebeck coefficient and resistivity were measured on single-crystal specimens as functions of temperature from about 80°K to about 300°K. Measurements of resistivity and Seebeck coefficient were made along the c-axis (perpendicular to the principal cleavage plane) on all specimens. In order to determine the effects of doping on the degree of anisotropy of the thermoelectric properties, measurements also were made perpendicular to the c-axis (parallel to the principal cleavage plane) on a few specimens. All electrical data presented in the following figures were obtained by measurement along the c-axis except where noted otherwise.

Electrical contact was made to the specimens with In-Bi eutectic solder. The solder was applied with a soldering pencil at as low a temperature as possible to prevent attack of the specimens by the solder.

The data obtained on the undoped (n-type) Bi-Sb alloys are shown in Figures 5 and 6 and in Table 5. Of the four compositions studied (5, 8, 12, and 14.6 atomic percent antimony), the specimen containing 8 percent antimony had the highest value of S^2/ρ over most of the temperature range covered. The alloys containing 5 and 14.6 atomic percent antimony had the lowest S^2/ρ values. The value of S^2/ρ for all alloys increased with decreasing temperature. Likewise, the figure of merit of these alloys increases with decreasing temperature. The figure of merit of n-type, undoped $Bi_{85.4}Sb_{14.6}$ specimen increased from 0.93×10^{-3}/°K at 300°K to 3.8×10^{-3}/°K at 80°K (Table 5). Similar behavior has been noted at Battelle and elsewhere in alloys containing 5 and 12 percent antimony. The opposite trend with temperature is observed in Bi_2Te_3 alloys, for which the figure of merit decreases two- to threefold from room temperature to 80°K.

TABLE 5. THERMOELECTRIC PROPERTIES OF $Bi_{85.4}Sb_{14.6}$ ALLOY

Specimen	Temp, °K	Seebeck Coefficient, μV/°K	Resistivity, ohm-cm	Thermal Conductivity, watt/cm-°K	Figure of Merit, $°K^{-1}$
20195-1	300	$76._8$	1.70×10^{-4}	$3.7_4 \times 10^{-2}$	0.93×10^{-3}
	80	$121._2$	1.64×10^{-4}	$2.3_7 \times 10^{-2}$	3.8×10^{-3}

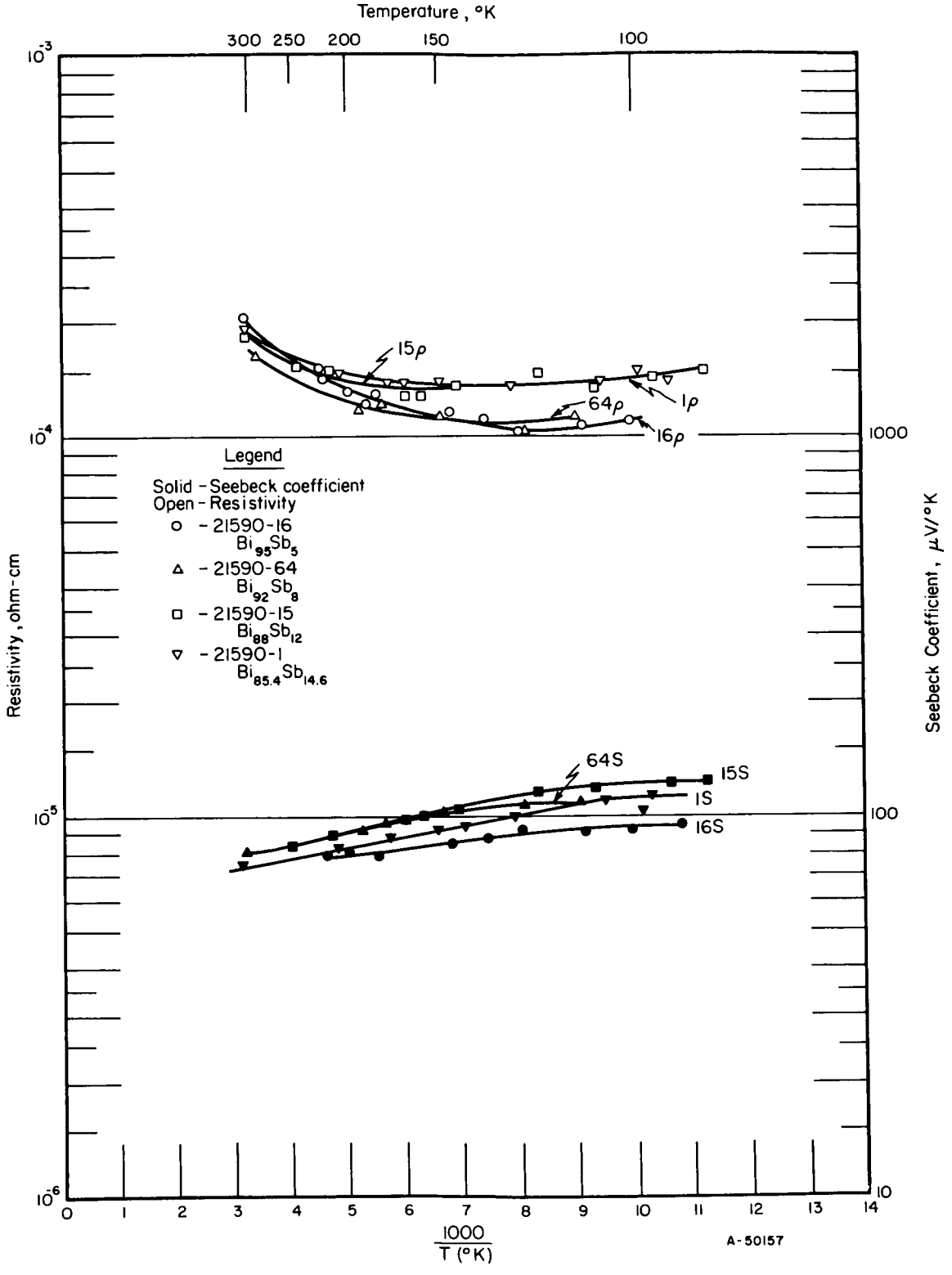

FIGURE 5. SEEBECK COEFFICIENT AND RESISTIVITY VERSUS RECIPROCAL TEMPERATURE FOR n-TYPE, UNDOPED Bi-Sb ALLOYS

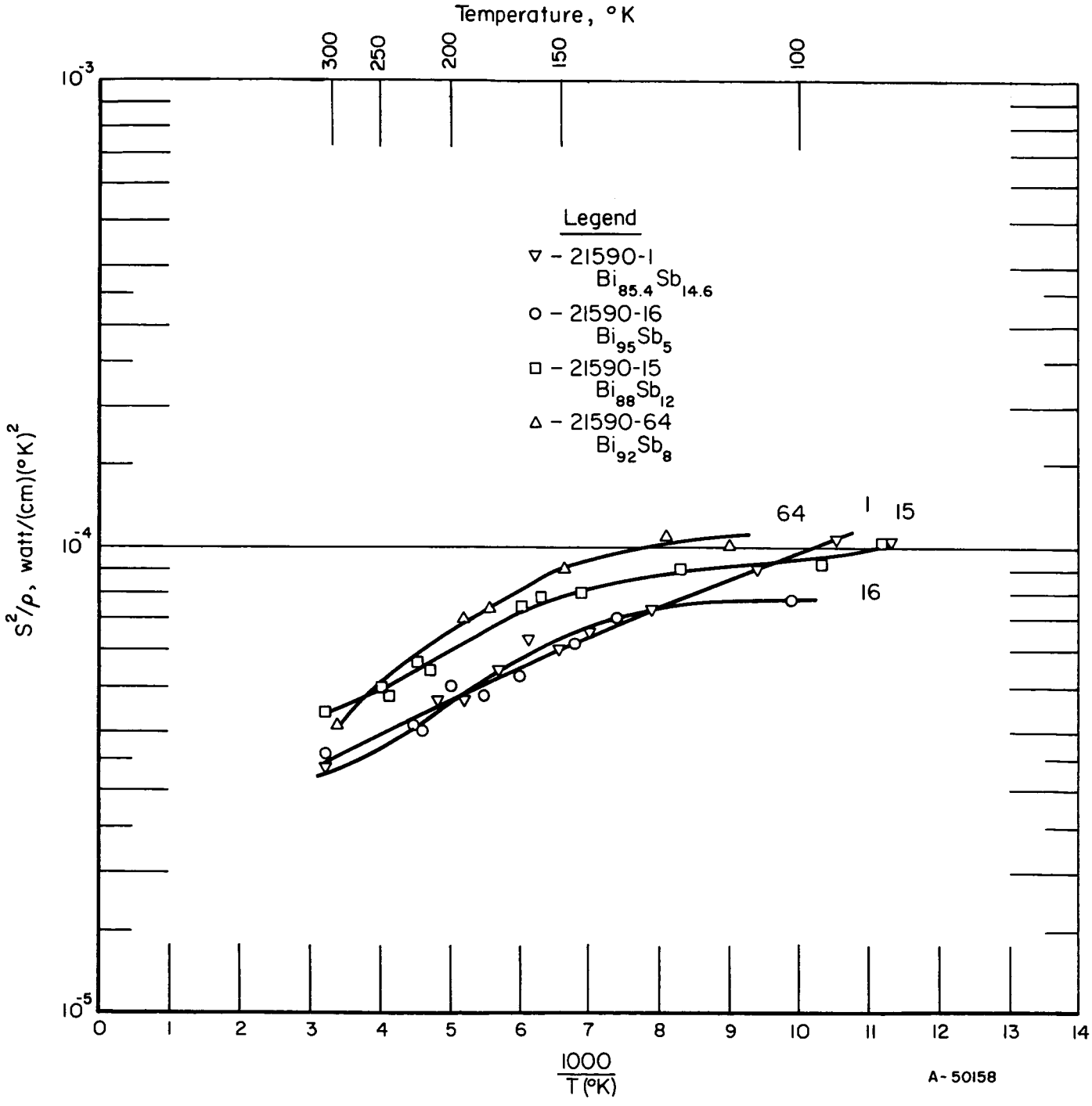

FIGURE 6. S^2/ρ VERSUS RECIPROCAL TEMPERATURE FOR n-TYPE, UNDOPED Bi-Sb ALLOYS

A number of $Bi_{86}Sb_{14}$ and $Bi_{88}Sb_{12}$ alloys were doped with varying concentrations of tellurium, which behaves as a donor (n-type dopant) in the Bi-Sb alloy system. The tellurium concentration was varied from 0.037 to 1.8 atomic percent in the $Bi_{86}Sb_{14}$ alloy. For comparison, the $Bi_{88}Sb_{12}$ alloy was doped with 0.038 atomic percent tellurium.

Most of the n-type tellurium-doped specimens, especially those containing more than 0.07 atomic percent tellurium, had very low Seebeck coefficient and S^2/ρ values (Figures 7 and 8) compared to those of the n-type, undoped alloys with the same nominal composition. This observation, combined with the fact (discussed below) that light p-type doping increases the values of S and S^2/ρ, indicates that the optimum electron concentration is lower than that in intrinsic material.

Tin was used as a p-type dopant in Bi-Sb alloys. Although tin behaves as an acceptor, a certain minimum concentration is required to make p-type conduction dominant at a given temperature. Below this concentration, the alloys are n-type (Curves 49, 49B, and 73 on Figure 9). Also, in a lightly doped material conduction may be predominantly by holes ($S > 0$) at low temperatures but by electrons ($S < 0$) at higher temperatures. The "crossover temperature" ($S = 0$) is dependent on tin concentration. The crossover behavior may be seen in Seebeck-coefficient Curves 27, 47, and 58 on Figure 9. Values of S^2/ρ for these specimens are shown in Figure 10.

A preliminary study was made of the anisotropy of the Seebeck coefficient and resistivity in doped Bi-Sb alloys. In n-type, undoped $Bi_{88}Sb_{12}$ alloy (Figure 11), the Seebeck coefficient is higher and the resistivity is lower along the c-axis rather than perpendicular to it. This results in higher S^2/ρ values along the c-axis. A similar behavior was observed in the $Bi_{86}Sb_{14}$ alloy containing 0.2 atomic percent tin on both the n-type and p-type sides of the crossover point. However, in the more heavily doped alloy (1.9 atomic percent tin), the Seebeck coefficient was higher and resistivity was lower perpendicular to the c-axis (Figure 12). For example, at 200°K, the values of Seebeck coefficient and resistivity were 62 μV/°K and 3.5 ohm-cm perpendicular to the c-axis ($S^2/\rho = 1.1 \times 10^{-5}$ watt/cm-°K^2) compared to 44 μV/°K and 5.5 ohm-cm along the c-axis ($S^2/\rho = 0.4 \times 10^{-5}$ watt/cm-°K^2). These S^2/ρ values, although the highest obtained thus far in p-type Bi-Sb alloys, are still an order of magnitude too low. It appears improbable that p-type Bi-Sb alloys will be useful for thermoelectric cooling. However, the n-type, tin-doped alloys show promise for use as thermoelectric materials at temperatures up to the vicinity of 300°K. From the data presented in Figure 10, it may be seen that the alloys containing nominally 0.04 and 0.08 atomic percent tin have higher S^2/ρ values at 300°K than the n-type, undoped $Bi_{86}Sb_{14}$ alloy. At 300°K, the $Bi_{85.7}Sb_{14.3}Sn_{0.04}$ alloy had an S^2/ρ value of 4.8×10^{-5} watt per cm-°K^2 compared to about 3.8×10^{-5} watt per cm-°K^2 for the undoped $Bi_{85.4}Sb_{14.6}$ alloy (for which $Z = 0.93 \times 10^{-3}$/°K – Table 5). Furthermore, in view of the higher resistivity of the doped material, its thermal conductivity is expected to be lower than that of the undoped alloys.

A significant improvement in S^2/ρ values of n-type $Bi_{88}Sb_{12}$ apparently was attained by doping with 0.08 mol percent CuBr (Figure 13). For the single CuBr-doped specimen prepared, values of 6.1×10^{-5} and 18×10^{-5}, watt/cm-°K^2 were measured at 300 and 80°K, respectively. These values are the highest measured to date on this project for any Bi-Sb alloy specimen. For comparison, the S^2/ρ values for an n-type, undoped $Bi_{88}Sb_{12}$ specimen were 4.5×10^{-5} and 10.2×10^{-5} watt/cm-°K at 300 and 90°K. The thermal conductivity of the CuBr-doped specimen has not been measured; assuming

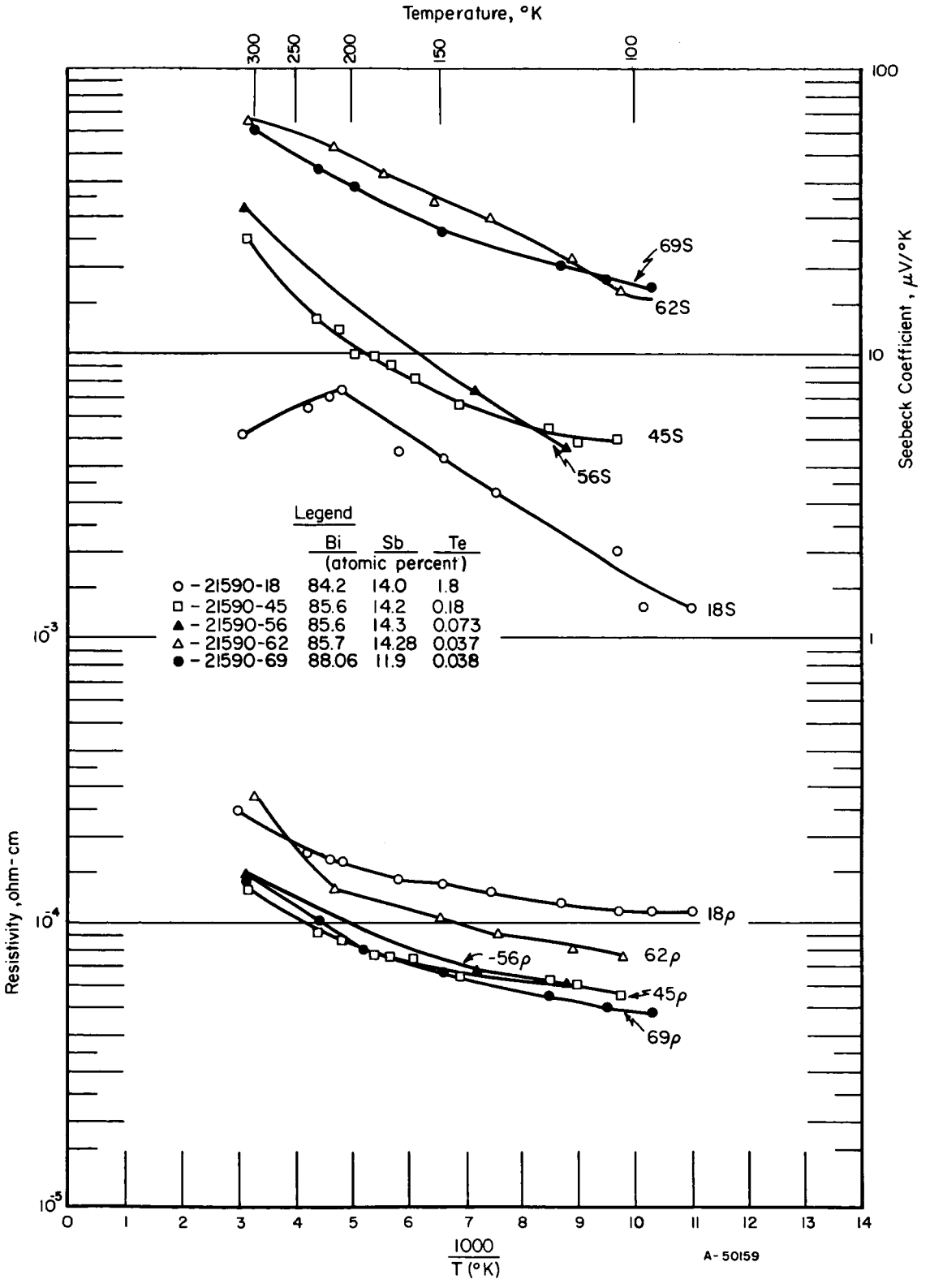

FIGURE 7. SEEBECK COEFFICIENT AND RESISTIVITY VERSUS RECIPROCAL TEMPERATURE FOR n-TYPE, TELLURIUM-DOPED Bi-Sb ALLOYS

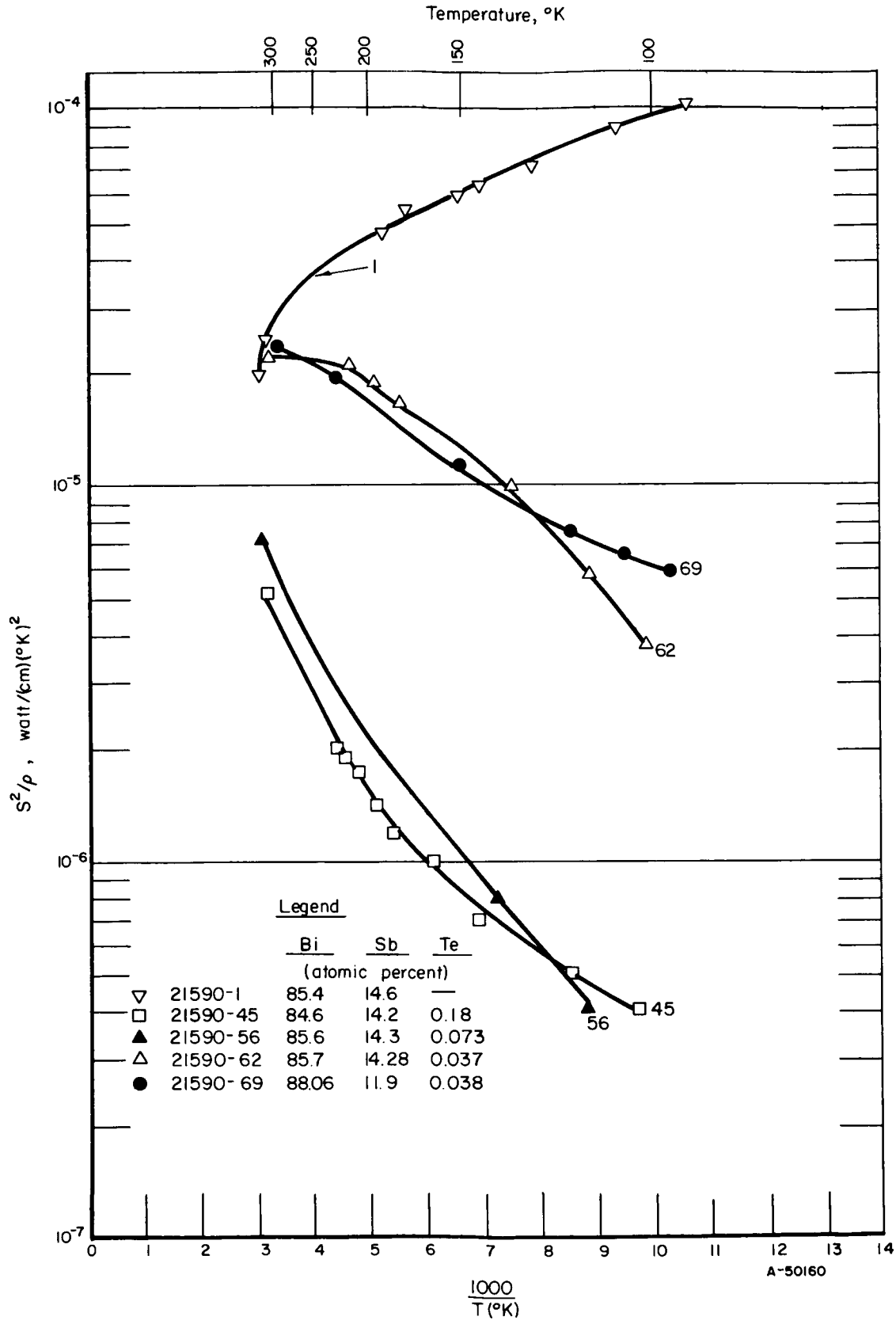

FIGURE 8. S^2/ρ VERSUS RECIPROCAL TEMPERATURE FOR n-TYPE, TELLURIUM-DOPED Bi-Sb ALLOYS

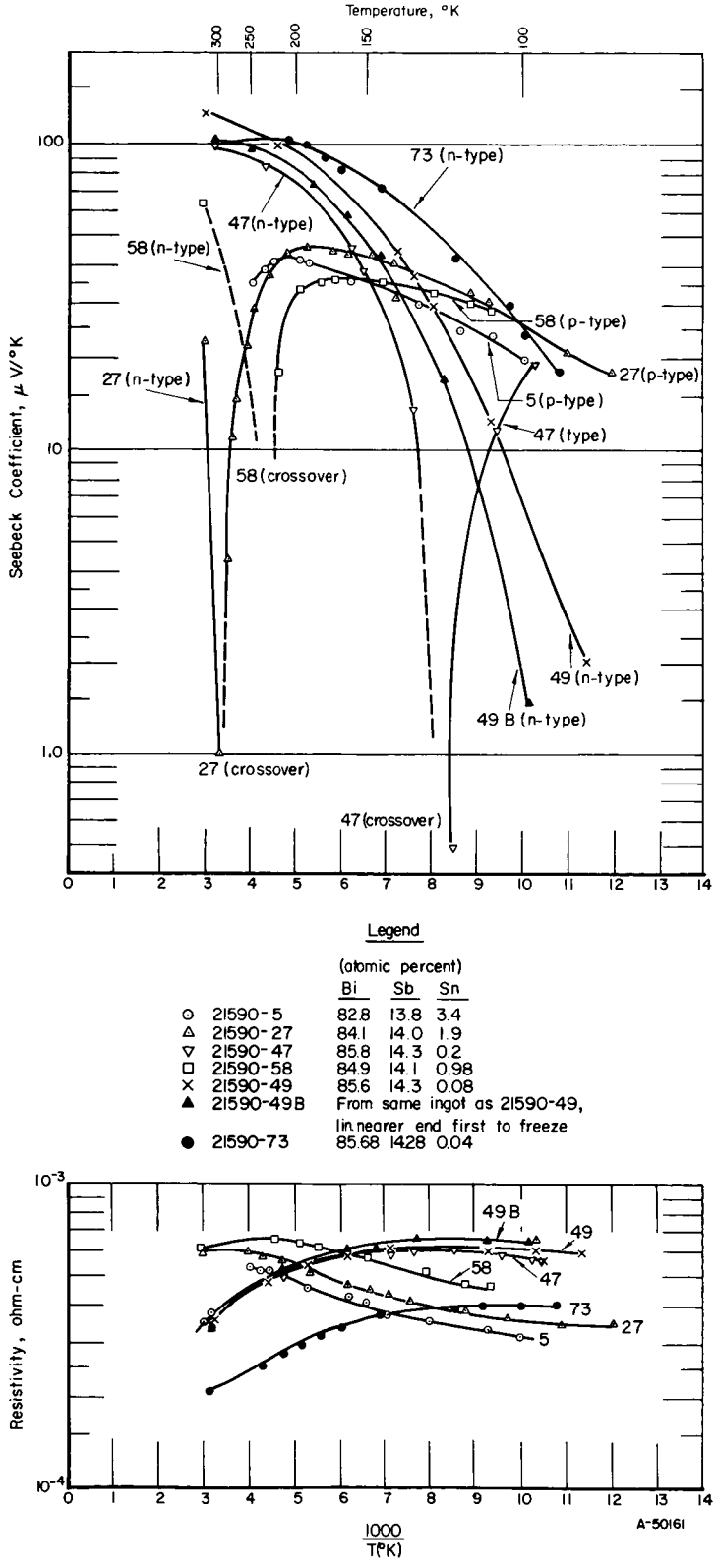

FIGURE 9. SEEBECK COEFFICIENT AND RESISTIVITY VERSUS RECIPROCAL TEMPERATURE FOR TIN-DOPED $Bi_{86}Sb_{14}$ ALLOYS

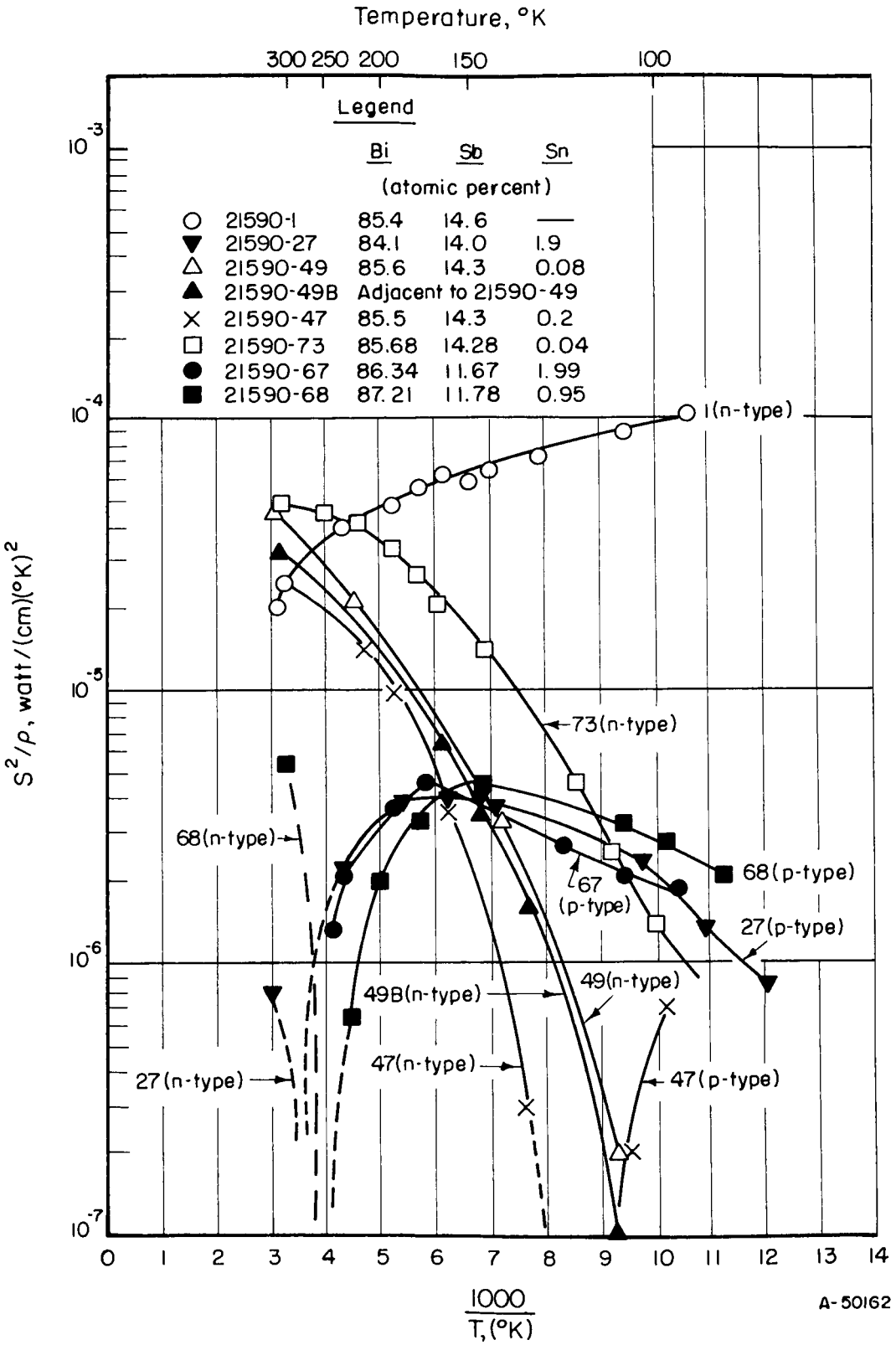

FIGURE 10. S^2/ρ VERSUS RECIPROCAL TEMPERATURE FOR Bi-Sb ALLOYS (Sn DOPED)

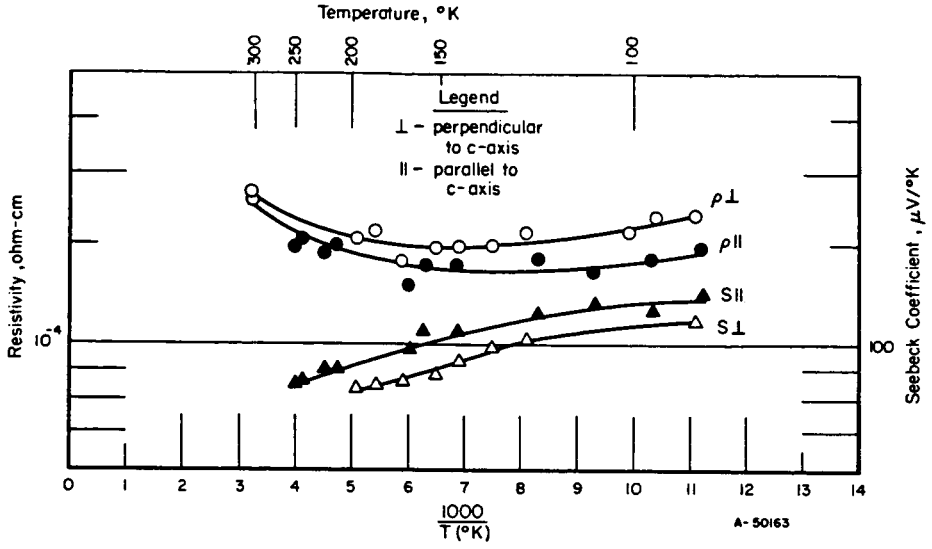

FIGURE 11. ANISOTROPY OF SEEBECK COEFFICIENT AND RESISTIVITY OF n-TYPE UNDOPED $Bi_{88}Sb_{12}$ ALLOY (21590-15)

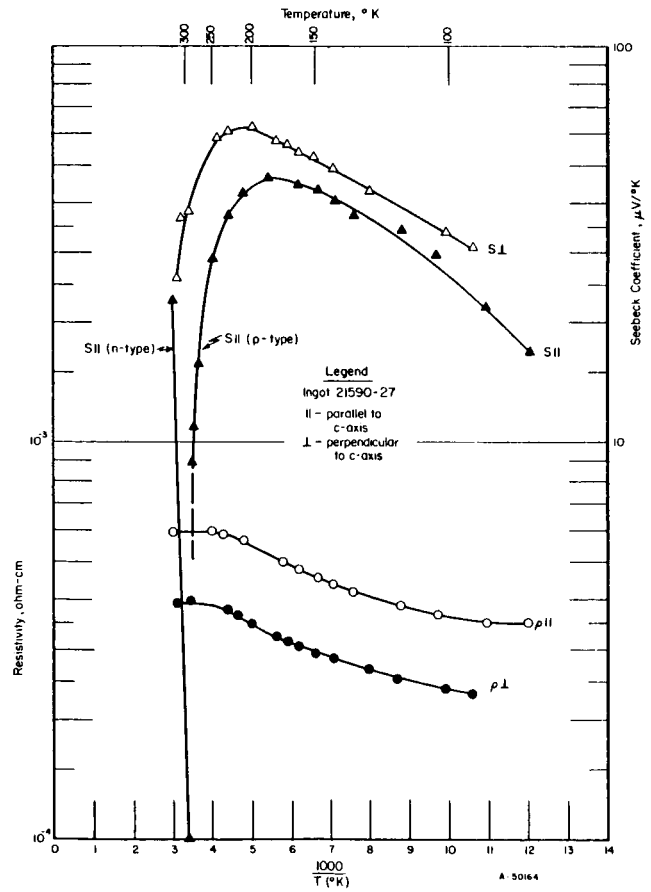

FIGURE 12. ANISOTROPY OF SEEBECK COEFFICIENT AND RESISTIVITY OF p-TYPE $Bi_{84.1}Sb_{14.0}Sn_{1.9}$ ALLOY

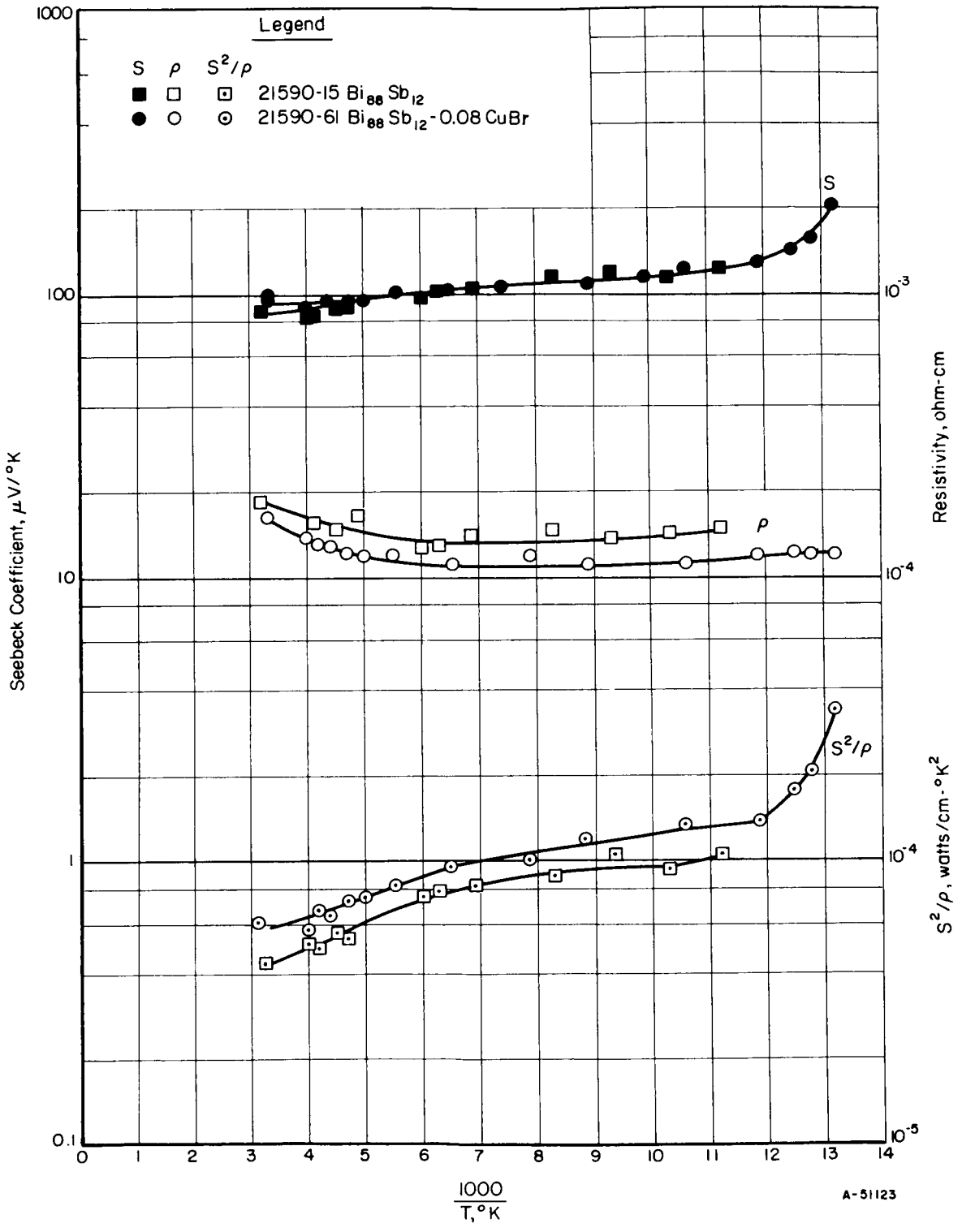

FIGURE 13. SEEBECK COEFFICIENT, RESISTIVITY AND S^2/ρ VERSUS RECIPROCAL TEMPERATURE FOR n-TYPE (DOPED AND UNDOPED) $Bi_{88}Sb_{12}$ ALLOYS

the same values as those for undoped $Bi_{85.4}Sb_{14.6}$ (Table 5) gives Z values of 1.6×10^{-3} and 7.5×10^{-3}/°K at 300 and 80°K, respectively.

Homogeneity. A high degree of inhomogeneity in a material generally leads to a lower figure of merit than if the material is homogeneous. The lower figure of merit for an inhomogeneous material results from an increase in the thermal conductivity and a decrease in the Seebeck coefficient by the circulating-current effect, as discussed earlier in this report. Thus, it is to be expected that the figure of merit of a material can be improved by improving the degree of homogeneity.

In several alloy systems – including the Bi-Sb system – it has been observed that single crystals exhibit a cellular-like structure. In a series of decanting and etching studies along with electron-microprobe analyses conducted on the $Bi_{95}Sb_5$ alloy at Battelle, it was determined that this cellular-like structure represents a high degree of inhomogeneity. The center of the cells, triangular pyramids extending from the crystallizing interface into the melt, is richer in antimony than the cell walls.

During this contract period, preliminary metallographic examinations were made of several $Bi_{86}Sb_{14}$ alloy specimens, doped and undoped, to determine the degree of inhomogeneity present*. Examinations were conducted on the cleavage plane (plane perpendicular to the trigonal axis).

Each of the specimens was found to contain randomly oriented cells. From the structures on the etched surfaces, as seen in Figure 14, some of the cells appeared to

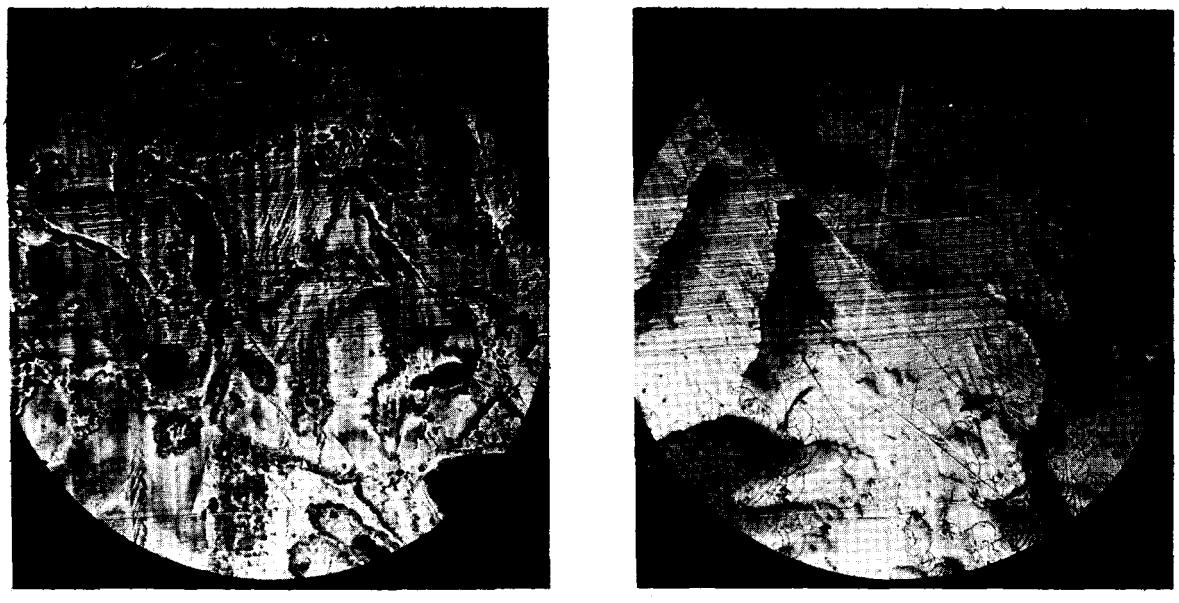

a. Cells Perpendicular to Cleavage Plane, 150 X

b. Cells Not Perpendicular to Cleavage Plane, 150 X

FIGURE 14. CELLULAR GROWTH IN Bi_{86} Sb_{14} ALLOYS

*The alloy specimens were examined by an electrolytic etching technique[10, 11]. Single-crystal cleaved specimens were mounted in Kold-Weld potting compound and mechanically polished. The polished specimens were then electrolytically etched, using a mixture of 20 parts methyl alcohol, 5 parts H_2SO_4, 5 parts HCl, and 2 parts ethylene glycol as the electrolyte. The etched surface was then electrolytically stained, using a 5 percent aqueous chromic acid solution as the electrolyte. Platinum was used as the electrodes. Contact was made to the specimens with the platinum anode.

be oriented perpendicular to the cleavage plane (two triangular structures in the lower half of Figure 14a), whereas other cells within the same specimen appeared to be oriented at some other angle (cross hatch in Figure 14b). This cellular-like structure represents a degree of inhomogeneity which may have a detrimental effect on the electrical properties of the alloys. Thus, improving the homogeneity of the alloys as well as the degree of crystal perfection may result in further improvement in the thermoelectric properties.

Theoretical Investigation

Introduction

The primary objective of the theoretical-investigation phase of this research program is to establish useful criteria for the selection or development of improved thermoelectric materials.

The quantitative rating of a given material for thermoelectric applications is the value of its dimensionless figure of merit ZT, where $Z \equiv S^2 \sigma/K$ is the figure of merit as ordinarily defined and T, S, σ, and K are the absolute temperature, Seebeck coefficient, electrical conductivity, and thermal conductivity, respectively. The various performance indices of thermoelectric power generators and heat pumps are usually functions of ZT rather than of Z alone.

The value of ZT for a given material is a function of its alloy composition, impurity doping, temperature, current direction with respect to crystallographic axes for noncubic crystals, magnetic field intensity and direction, state of mechanical stress, and degree of compositional homogeneity. It would be almost meaningless for the purpose of rating materials to measure the value of Z of only a single specimen of a material under a particular set of values of these variables. For example, a specimen of even one of the best thermoelectric materials could have $S \approx 0$ and hence $ZT \approx 0$. A vanishingly small value of the Seebeck coefficient could correspond to either greatly overdoping with an acceptor impurity, greatly overdoping with a donor impurity, or by doping to the neighborhood of the crossover point between negative and positive Seebeck coefficient, which is not necessarily the same point as that for compensated material as determined by a Hall coefficient measurement. The only meaningful way to rate the thermoelectric merit of a given material would be to ascertain the maximum value of ZT attainable by optimizing this material with respect to all variables of interest over their feasible ranges of variation.

Since ZT is a dimensionless quantity, its maximum value when optimized with respect to all the variables of interest would have to be a function of certain dimensionless combinations of measures of the various intrinsic properties of the material. These combinations are termed the "basic material parameters". Once these basic material parameters have been identified, measurements on a given material to determine its thermoelectric quality should be devised for the purpose of determining the value of a sufficient number of them to permit at least an upper limit to the maximum value of ZT for that material to be estimated. If this upper limit is high enough to be of interest, further measurements would be in order to determine the value of the maximum ZT more precisely. The criteria for finding or making improved thermoelectric materials would thus be the attainment of more favorable values or more favorable combinations of values of these basic material parameters.

Each scientific discipline purporting to account for some aspect of solid-state behavior can be characterized by its own set of basic material parameters, compounded from the various constants that appear in the analytical models assumed for that discipline. Conceivably, dimensionless material parameters could also be formulated from interdisciplinary approaches, based on combinations of disciplines. The most useful set of basic material parameters would be that set which consists of the smallest number of independent parameters with which the maximum attainable value of ZT for a material could be correlated in the most direct and simplest manner. This correlation should preferably, but not necessarily, be capable of being determined by analytical methods. A fairly good empirical correlation of the maximum ZT with a single parameter, or at most two parameters, would probably be of greater value for use as a selection criterion than an analytically obtained correlation with several parameters that may not be completely independent of one another and that may exhibit counteracting effects on the maximum attainable value of ZT.

The Electron-Energy-Band Model

The scientific discipline based on the electron-energy-band model of the electrical and thermoelectric behaviors of semiconductors has permitted the identification of several basic material parameters whose functional relationship to the maximum value of ZT have been ascertained by numerical analyses performed with the aid of a digital computer. This functional relationship is the only one known at present. It may furnish clues for finding more useful material-selection criteria based on other disciplines, if such exist. These possibilities will be discussed in appropriate places throughout the text of this report.

Optimizations of ZT with respect to magnetic field intensity, mechanical stress, and compositional homogeneity are not considered in this report. The maximum value of ZT can occur at a zero, intermediate, or strong magnetic field depending upon the band structure, magnetic field and current orientations, Fermi energy, and other factors[12]. Application of uniaxial or triaxial stress can have profound effects on the various band-structure and transport parameters, in particular on the energy differences between the various band edges and on otherwise equivalent extrema of the same energy band[13]. Changes in ZT resulting from stress application may be favorable or unfavorable, depending upon circumstances to be discussed later in this report. Compositional inhomogeneities are usually undesirable because of the deleterious effects of the resulting circulating currents. The beneficial gradients or step changes in composition that may be incorporated along the legs of thermocouples are related to the fact that the optimum composition is a function of temperature.

Although special cases might exist for which definite advantages might be obtained by applying a magnetic field or stress, ordinary applications of interest would correspond to the absence of a magnetic field or stress. Thus, the optimizations of ZT with respect to the other parameters discussed in this report are assumed to be for stress-free, compositionally homogeneous material in zero magnetic field. Work in the future might be undertaken to delineate more closely the circumstances and material properties for which the increase in ZT obtainable by application of a magnetic field or stress might outweigh the disadvantages involved.

Single-Band Conduction. Electrical conduction in a single energy band, either a single conduction band for n-type materials or a single valence band for p-type materials,

is the approximation that is usually made in the literature for studying the relationship between the thermoelectric figure of merit and the material variables. This approximation is a good one for many materials of practical interest since the optimum doping is usually such as to bring the Fermi energy within about ±1 kT from the band edge. However, for temperatures such that the energy gap between conduction and valence bands drops below about 4 to 8 kT, depending upon the values of the material parameters of the two bands[1, 2], intrinsic conduction effects become sufficiently great to invalidate the single-band approximation.

As discussed in the First Quarterly Progress Report, Z(max)T, the value of ZT as optimized with respect to impurity doping only, is a function of only two basic material parameters, r and β, for single-band conduction. The quantity r is the exponent in the assumed power-law relationship between the mean free path of the charge carrier and its energy, with r = 0 for predominantly acoustic-mode lattice vibration scattering, r = 1 for predominantly optical-mode lattice vibration scattering, and r = 2 for scattering predominantly by ionized impurity centers. The quantity β is the basic material parameter, composed of a dimensionless combination of a number of physical constants as follows:

$$\beta \equiv (k/e)^2 \, \sigma_o T/K_L \quad , \tag{1}$$

where

$$\sigma_o = N \, 2(2\pi \, m_d \, kT/h^2)^{3/2} \, e\mu_c \tag{2}$$

and

$$\mu_c = \frac{1}{N} \sum_{i=1}^{N} (\lambda_{1i}^2 \, \mu_1 + \lambda_{2i}^2 \, \mu_2 + \lambda_{3i}^2 \, \mu_3) \quad . \tag{3}$$

In Equation (1), k/e is the ratio of Boltzmann's constant to the charge on the electron and K_L is the lattice component of the thermal conductivity in the current direction. In Equation (2), N is the number of equivalent extrema of the energy band in question, m_d is the density-of-states mass in the neighborhood of each equivalent valley, and h is Planck's constant. In Equation (3), the low-carrier-concentration value of the charge-carrier mobility, μ_c, is expressed as a function of the "partial mobilities", μ_1, μ_2, and μ_3 associated with conduction along the principal-axes directions of the energy ellipsoid for charge carriers in the neighborhood of each extremum[14], where λ_{1i}, λ_{2i}, and λ_{3i} are the direction cosines of the three respective principal axes for the i-th extremum with respect to the current direction.

The theory that leads to the above results is given by Chasmar and Stratton[15]. Briefly summarized, expressions for S, σ, and K are first formulated in terms of the physical constants pertinent to the assumed parabolic relationship between energy and wave-number vector and the value of the reduced Fermi energy, η, as measured from the band edge. When these are combined to form $ZT = S^2\sigma T/K$, it is seen that ZT is a function only of r, β, and η. Optimization with respect to η, which is accomplished numerically, results in Z(max)T as a function of r and β. This functional relationship is represented in the form of Z(max)T versus β exp r for r = -1, 0, 1, and 2 in Figure 15 to show that in the neighborhood of $Z(max)T \approx 1$, which corresponds to about the best thermoelectric materials presently available, Z(max)T is a function only of the single parameter β exp r to a good approximation.

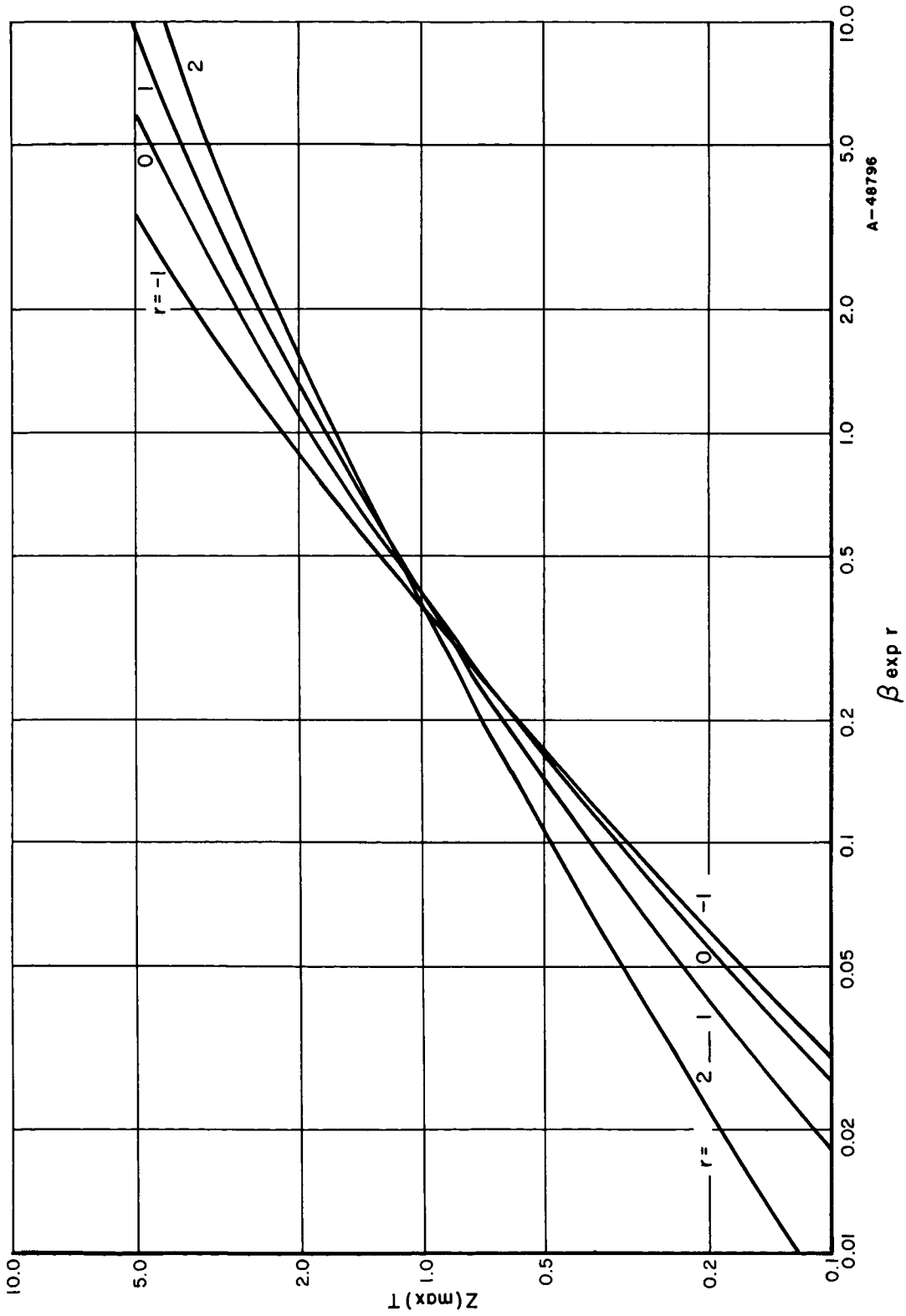

FIGURE 15. Z(max)T AS A FUNCTION OF β exp r

The parameter β exp r contains the two factors σ_o exp r and K_L. The value of σ_o exp r is readily obtainable from measurements of the electrical conductivity and the Seebeck coefficient on the same specimen of the material of essentially single-band extrinsic conductivity, as previously explained in this report. If the thermal conductivity is also measured, K_L can be obtained by subtracting the electronic contribution, which is related to the electrical conductivity by the Wiedeman-Franz-Lorenz law. Consequently, the value of β exp r for a given material, and hence the value of Z(max)T for that material, can be determined from measurements of the very same quantities, S, σ, and K that enter that enter into the definition of the magnitude of Z for a specimen of that material. Curves for estimating the value of Z(max)T from measured values of the quantities S and $K/\sigma T$ are given in Reference (16).

Two-Band Conduction. As pointed out in the Second Quarterly Progress Report, the single-band model is inadequate for obtaining the value of $(ZT)_{max}$, the value of ZT as optimized with respect to both impurity doping and temperature. At least a two-band model is needed, since it is the thermally activated minority carriers that limit the value of Z(max)T by their adverse effects on the Seebeck coefficient and on the thermal conductivity as the temperature is increased. It eventually becomes impossible to compensate for these effects by increasing the impurity doping to suppress the minority carriers since carrier concentration degeneracy also affects the Seebeck coefficient adversely. Consequently, the value of Z(max)T goes through the maximum value of $(ZT)_{max}$ as the temperature is increased despite the usually rapid increase in the value of β exp r with increasing temperature.

The ZT theory for the two-band model is given in Reference (2). This theory is summarized in the Second Quarterly Progress Report, as well as the analytical procedure for the numerical computation of Z(max)T. The value of Z(max)T for the two-band model is a function of four basic material parameters, r, β, γ, and η_G, if it is assumed that the same value of r applies to charge-carrier scattering in both bands. The quantity β is defined as in Equation (1), using the value of σ_o pertinent to the majority-carrier band, the conduction band for n-type material or the valence-band for p-type material. The parameter $\gamma \equiv (\beta_e/\beta_h)^{1/2} = (\sigma_{oe}/\sigma_{oh})^{1/2}$ for n-type material and its reciprocal for p-type material. The quantity η_G is the reduced band gap, positive for semiconductors and negative for semimetals.

Figure 16 shows Z(max)T as a function of β for r = 0 and Figure 17 shows the analogous function for r = 1, both with η_G and γ^2 as parameters. The uppermost curves in both figures marked "$\eta_G = \infty$ or $\gamma = \infty$" are the same as the single-band curves of Figure 15 for r = 0 and r = 1, respectively. The monotonic increase of Z(max)T with β predicted by the single-band model is replaced in the two-band model with a rapid leveling off" to constant asymptotic values of Z(max)T that are functions of η_G and γ as β increases indefinitely. These asymptotic Z(max)T values are plotted in Figure 12 of the Second Quarterly Progress Report as functions of r, η_G, and γ.

It is evident from Figures 16 and 17 that the greater the value of the material parameter β, the greater must be the actual magnitude of either η_G or γ for either of them to be effectively infinite; that is, for the single-band Z(max)T value to be approximated. This is one of the reasons why it is increasingly difficult to find thermoelectric materials with higher Z(max)T values; they must have higher values of both β and η_G or γ.

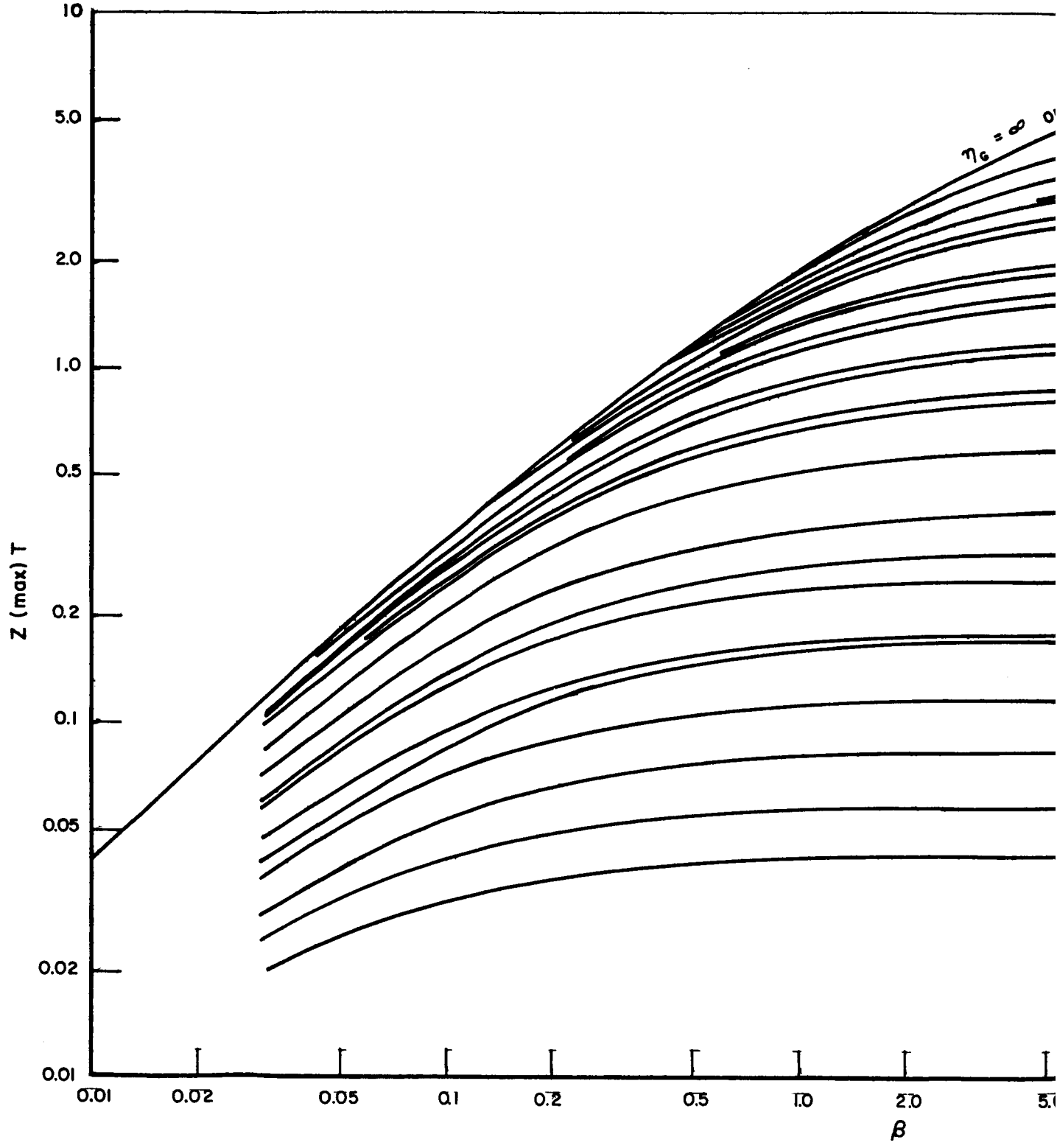

FIGURE 16. Z(max)T AS A FUNCTION OF β FOR r = 0 AND FOR VARIOUS VALUES FOR η_G AND γ

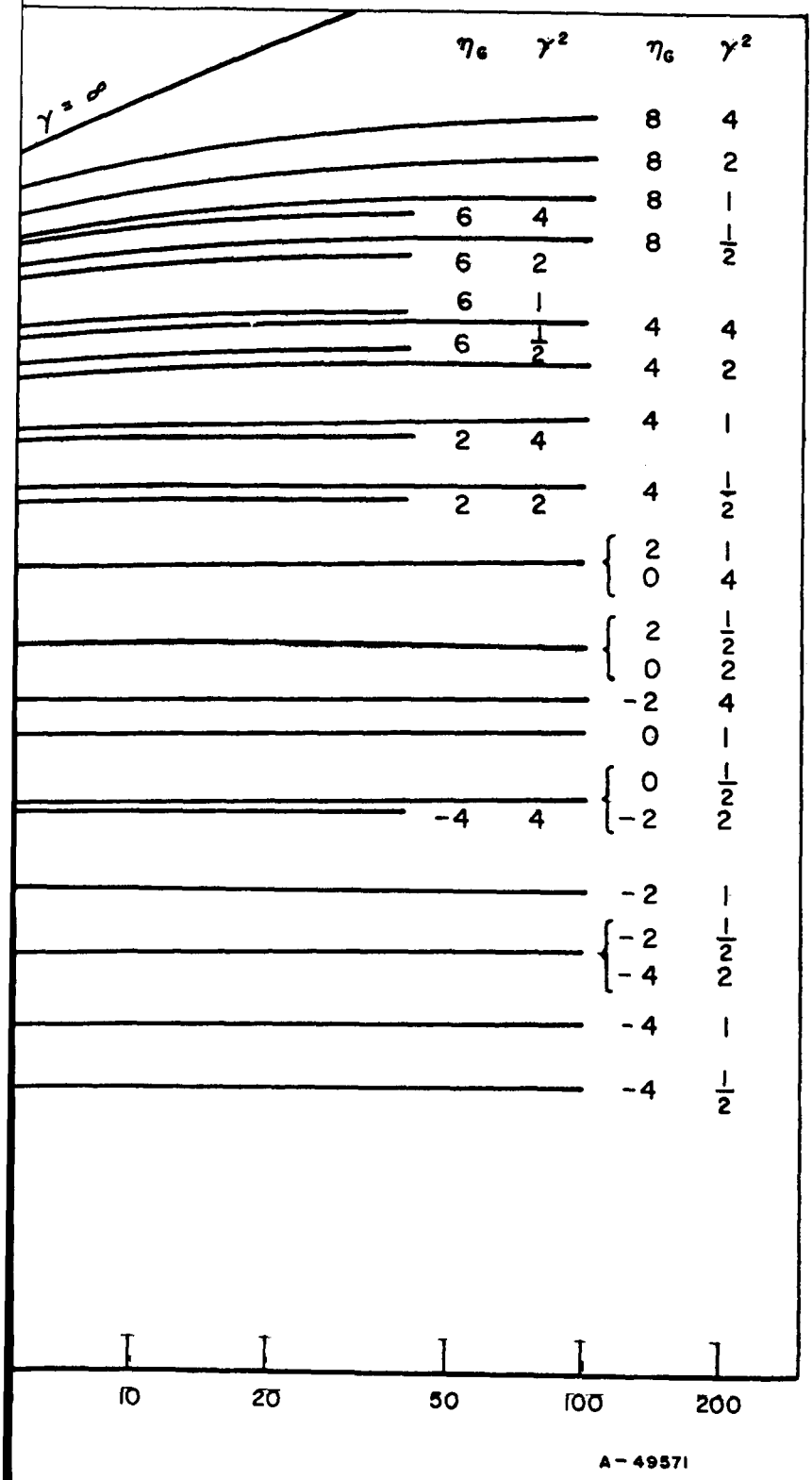
η_G γ^2
η_G γ^2
$\gamma = \infty$
8 4
8 2
8 1
6 4
8 $\frac{1}{2}$
6 2
6 1
4 4
6 $\frac{1}{2}$
4 2
4 1
2 4
4 $\frac{1}{2}$
2 2
2 1
0 4
2 $\frac{1}{2}$
0 2
-2 4
0 1
0 $\frac{1}{2}$
-4 4
-2 2
-2 1
-2 $\frac{1}{2}$
-4 2
-4 1
-4 $\frac{1}{2}$
10
20
50
100
200

A-49571

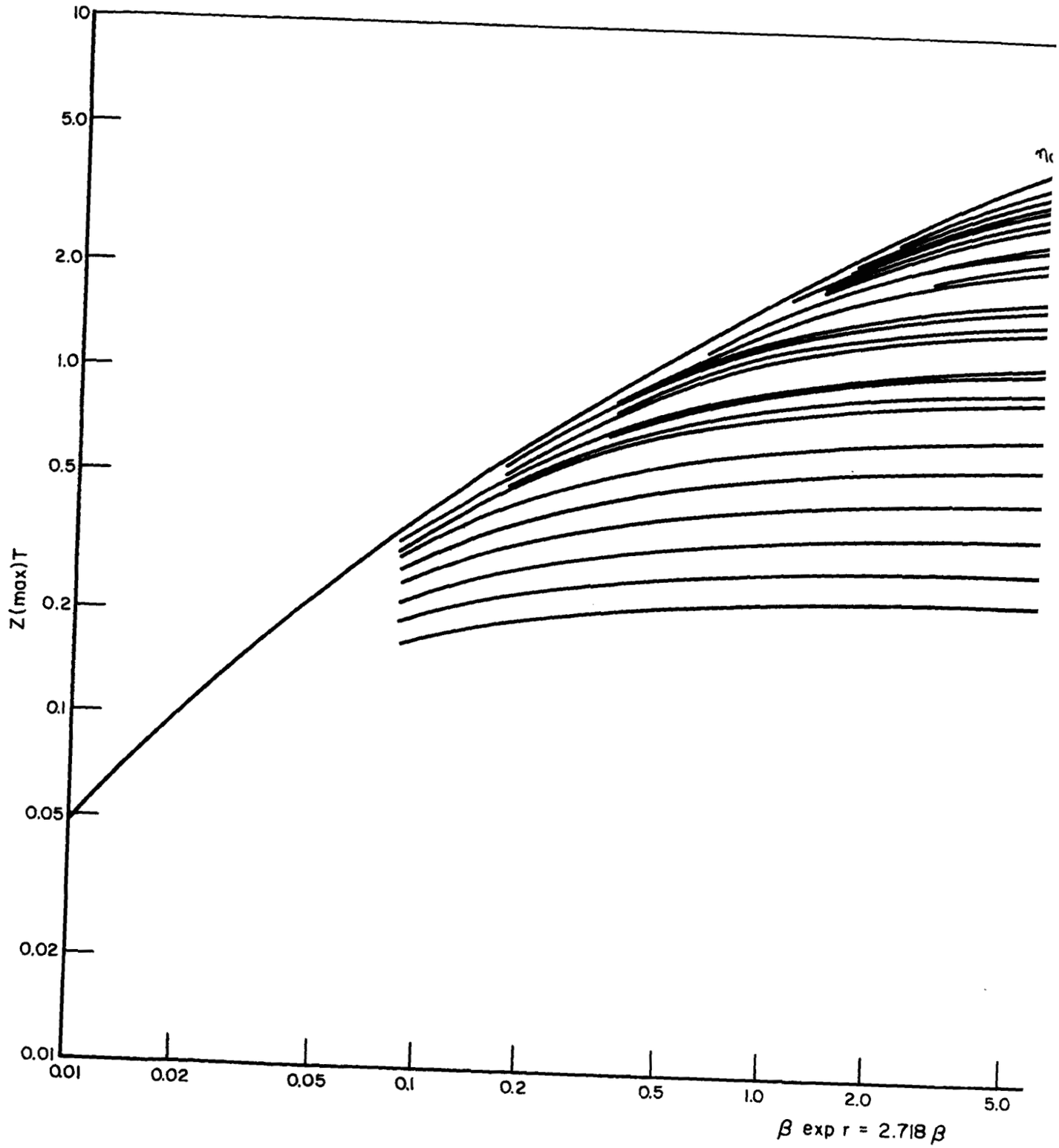

FIGURE 17. Z(max)T AS A FUNCTION OF β exp r FOR r = 1 AND FOR VARIOUS VALUES OF η_G AND γ

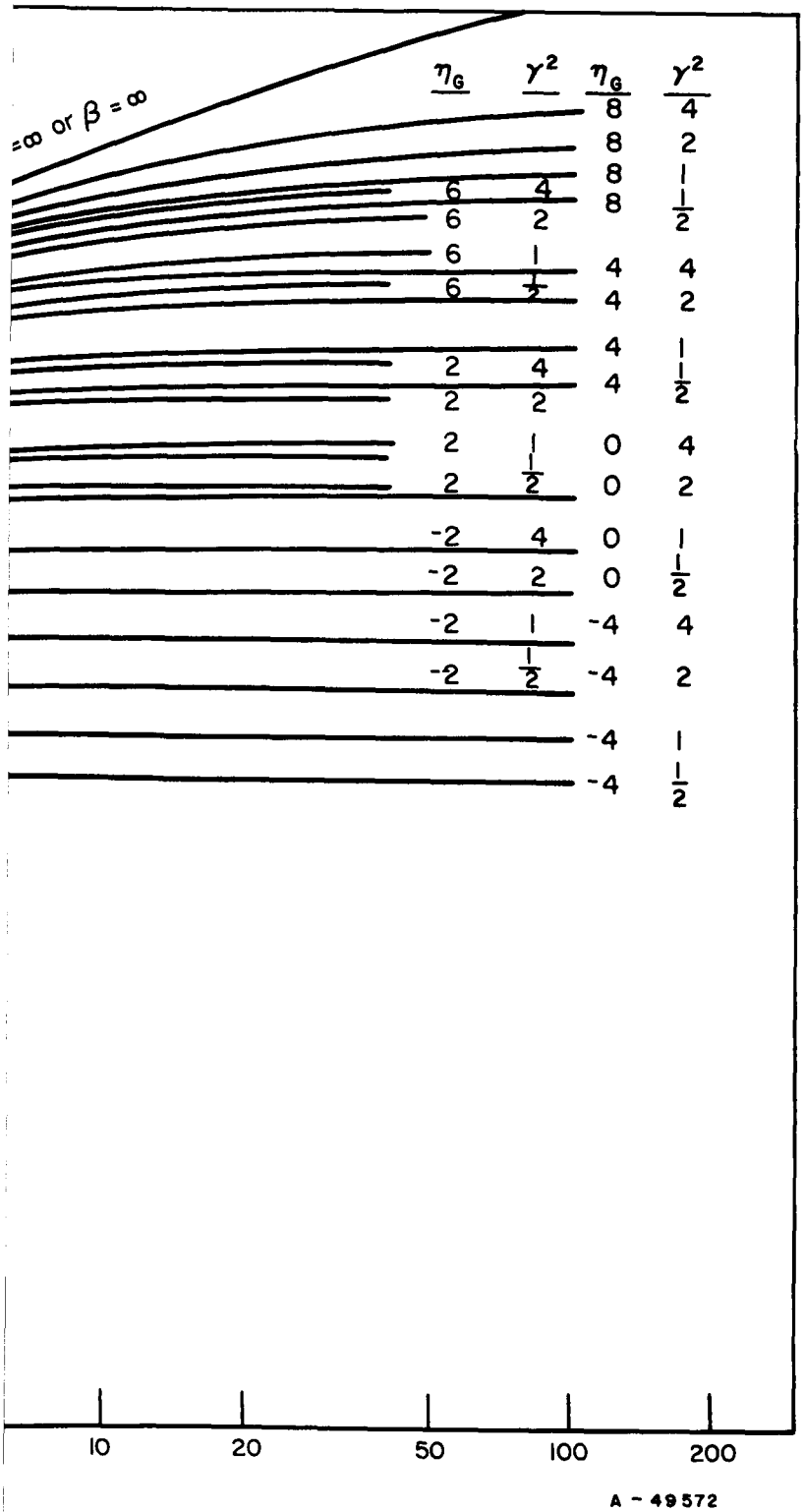
=∞ or β = ∞
η_G
γ^2
η_G
$\frac{\gamma^2}{4}$
8 8
8 2
8 1
6 4 8 $\frac{1}{2}$
6 2
6 1
6 $\frac{1}{2}$ 4 4
4 2
4 1
2 4 4 $\frac{1}{2}$
2 2
2 1 0 4
2 $\frac{1}{2}$ 0 2
-2 4 0 1
-2 2 0 $\frac{1}{2}$
-2 1 -4 4
-2 $\frac{1}{2}$ -4 2
-4 1
-4 $\frac{1}{2}$
10
20
50
100
200

A - 49572

With the aid of Figures 16 and 17 it is possible to assess more expeditiously the effectiveness of various measures taken to attempt to improve the ZT value of a given material. For example, alloying with an increasing percentage of a miscible compound may serve to increase β but to decrease η_G and γ. Use of the curves in these figures would then indicate if there would be any net gain or loss in the value of Z(max)T with increasing alloy composition. If there is an initial net gain, it could be determined what alloy composition, if any, would be optimum. Determination of the feasibility of obtaining optimum doping could then be made with the optimum alloy composition, assuming that the predicted Z(max)T value is high enough to justify further experimentation.

The solid lines of Figure 18 are contour curves of constant values of Z(max)T on a grid of β exp r versus $\eta_G + 2.89 \ln \gamma$ for r = 0, as obtained by cross-plotting the information on Figure 16. As shown in the Second Quarterly Progress Report, the asymmetry in the σ_o values of the two bands is approximately equivalent to an increase in band gap by $2.89 \ln \gamma$ ($2.31 \ln \gamma$ for r = 1) over a wide range of values of the various parameters. The $(ZT)_{max}$ considerations are facilitated by this replot. (The analogous replot for the case of r = 1 is not given in this report. It is given in Figure 14 of the Second Quarterly Progress Report.)

The broken-line curves on Figure 18 represent the loci of the points (η_G, $\beta + 2.89 \ln \gamma$) for various hypothetical materials as the temperature is changed and the doping adjusted to optimum at each temperature. For these broken-line curves it is assumed that $\gamma = 1$ and is independent of T, that m_d is independent of T, that μ_c varies as $T^{-3/2}$, and that K_L varies as T^{-1}. Consequently, β varies as T^2, in accordance with Equations (1) and (2). It is also assumed that η_G varies as T^{-1}, corresponding to neglect of the temperature dependence of the energy gap.

The value of $(ZT)_{max}$ for any given material corresponds to the point where the broken-line curve for that material becomes tangent to one of the curves of Z(max)T = constant. Thus, a hypothetical material with, say, room-temperature values of $\beta = 0.16$, $\gamma = 1$, $\eta_G = 16$ and Z(max)T = 0.50 (Point A on Figure 18) would be predicted to have a value of $(ZT)_{max}$ of slightly over 1.40 at $\beta = 0.90$ and $\eta_G = 6.7$, at a temperature of T = 300(2.45) = 730°K (Point B on Figure 18). It is assumed, of course, that no phase changes occur in the material when raising the temperature from that corresponding to Point A to that corresponding to Point B. It is also emphasized that the Z(max)T values corresponding to both Points A and B are the ZT values at optimum doping and not necessarily the actual ZT values of the same specimen of the material at these respective temperatures, since the optimum concentration of impurity doping at Point B may not necessarily be the same as that of Point A. These curves enable us to predict the potentialities of a given material at any temperature, subject to the limitations of phase stability and ability to obtain the proper dopant concentration at that temperature.

Consider the third broken-line curve from the left, the one that passes through the point $\eta_G + 2.89 \ln \gamma = 10$, $\beta = 0.01$ at the bottom of the figure. This curve is closely tangent to the Z(max)T = 0.35 solid curve over the range from about $\eta_G = 1.5$, $\beta = 0.4$ to about $\eta_G = 0.5$, $\beta = 3.6$. This represents a 3 to 1 range in T. On the other hand the broken-line curve on which Points A and B lie is tangent to the Z(max)T = 1.4 curve from about $\eta_G = 6.0$ to about $\eta_G = 7.2$, which is only about a 1.2 to 1 range in T. It is seen that the higher the value of $(ZT)_{max}$, the smaller is the temperature range over which Z(max)T = $(ZT)_{max}$. This observation is of evident technical importance in the design of thermocouple legs with the possibly improved materials of the future, since the better the material the more restricted is the temperature range over which it could

operate at $(ZT)_{max}$. The fact that the critical temperature range over which $Z(max)T = (ZT)_{max}$ becomes more restricted for the better materials may be another reason why it is so difficult to find improved materials.

Figure 18 could be used to predict the temperature behavior of Z(max)T and to find the value of $(ZT)_{max}$ for any real material, the loci of whose values of β and $\eta_G + 2.89 \ln\gamma$ might not necessarily run parallel to the family of broken lines on Figure 18 as the temperature is changed. In order to trace the locus of points of any real material it is necessary to know how μ_{ce} and μ_{ce}/μ_{ch} vary with temperature, the former for use in determining the temperature variation of σ_{oe} and the latter for determining the temperature variation of γ. The variations of m_{de} and m_{de}/m_{dh} with temperature at the optimum doping level would likewise be needed for the same purposes, if one or both energy bands are nonparabolic. The variation of energy gap with temperature must be known to obtain the correct temperature variation of η_G.

Multiband Conduction. In the $(ZT)_{max}$ analysis discussed above, the possible activation of additional energy bands with increase in temperature could not be taken into account with the two-band model. In addition, a multiband model for the Z(max)T and $(ZT)_{max}$ analyses would be of particular interest for alloys of elements or compounds whose corresponding primary bands are different. Well-known examples are silicon, whose primary conduction band consists of six valleys on the (100) axes, and germanium, whose primary conduction band consists of four valleys on the (111) axes. The (000) and (111) secondary conduction bands of silicon lie about 1.5 ev above the primary band edge,[17] and hence can clearly be neglected for all physical processes involving thermal activation of charge carriers (1.0 kT ≅ 0.026 ev at T = 300°K). The (000) and (100) minima for germanium lie only about 0.18 ev above the primary conduction band, however. As silicon atoms are substituted into the germanium lattice, the (000), (111), and (100) conduction band minima all move up in energy level relative to the (000) valence band maximum, but at decreasing rates in the order listed[18]. At about 14 percent silicon the (111) and (100) minima are at the same energy level[19]. Hence, both conduction bands must be taken into account in analyzing the thermoelectric behaviors of Si-Ge alloys with compositions in the neighborhood of this crossover point. Likewise, as will be discussed later, since the primary valence band of pure bismuth differs from that of pure antimony, a crossover point is to be expected for some Bi-Sb alloy composition. In the neighborhood of this crossover point, a three-band model would be appropriate because of the small energy difference between the conduction and valence band edges.

The general theory of ZT for multiband conduction and its application to two special cases of three-band conduction are outlined in the Third Quarterly Progress Report. One special case of three-band conduction consists of a single conduction band and a double valence band, with σ_{oh} representing the sum of the σ_o values for the two valence bands. As for the two-band model, $\gamma = (\sigma_{oe}/\sigma_{oh})^{1/2}$ and η_G is the energy gap between the conduction-band minimum and the primary (upper lying) valence-band maximum. η_{12} is the reduced energy difference between the two valence bands and the individual σ_o values of the primary and secondary valence bands are designated by $\epsilon\sigma_{oh}$ and $(1-\epsilon)\sigma_{oh}$, respectively. Another special case of the three-band model consists of a double conduction band but single valence band, with η_{12} now being the reduced energy difference between the primary, $\epsilon\sigma_{oe}$, and the secondary, $(1-\epsilon)\sigma_{oe}$, conduction bands. In both cases the value of Z(max)T for n-type material is a function of the six parameters r, η_G, γ, β_e, η_{12}, and ϵ. It is clear that the two additional cases of Z(max)T for p-type materials are thereby also covered by appropriate redefinition of γ as $(\sigma_{oh}/\sigma_{oe})^{1/2}$.

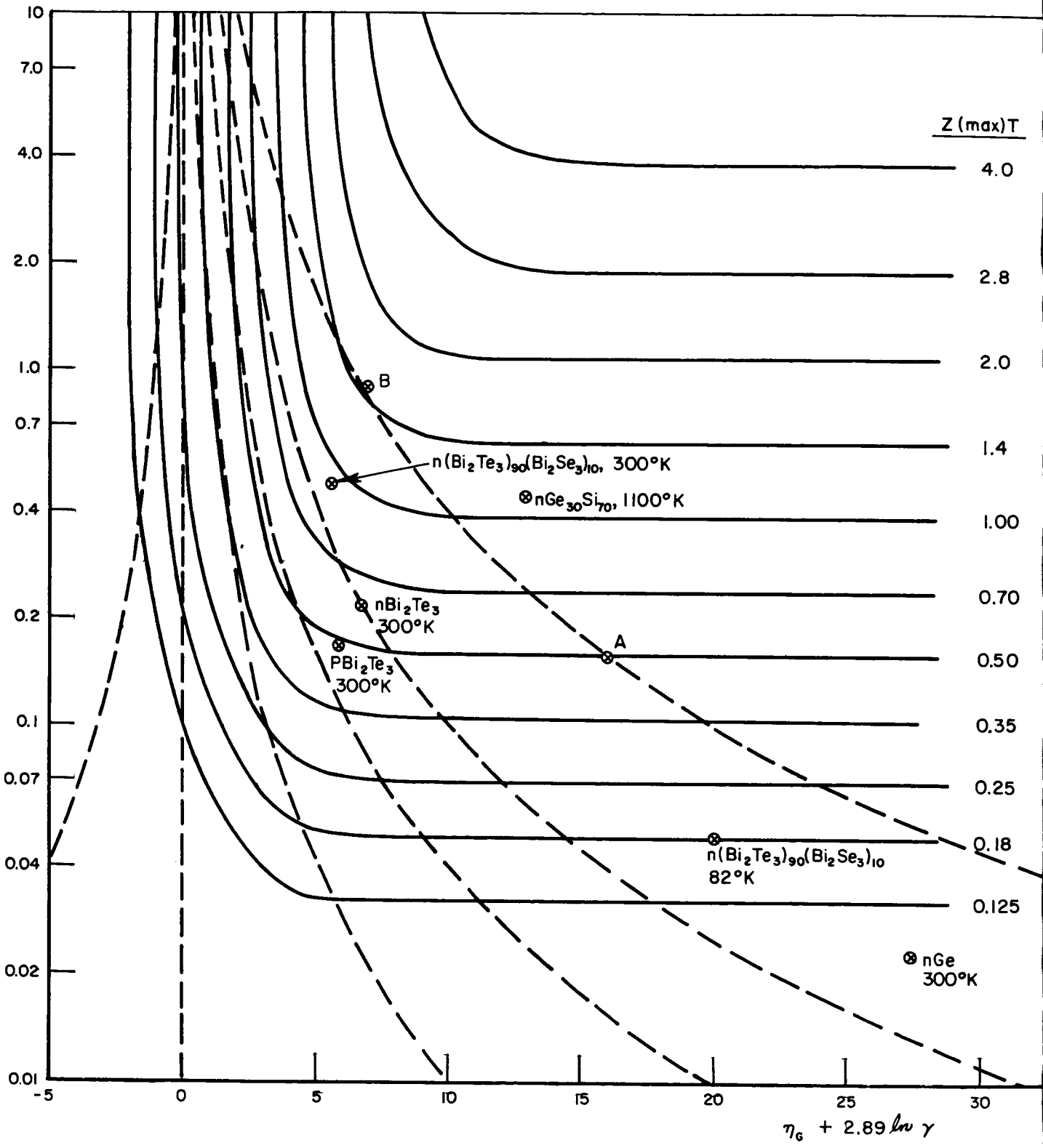

FIGURE 18. CONTOUR PLOT OF CONSTANT Z(max)T FOR r = 0

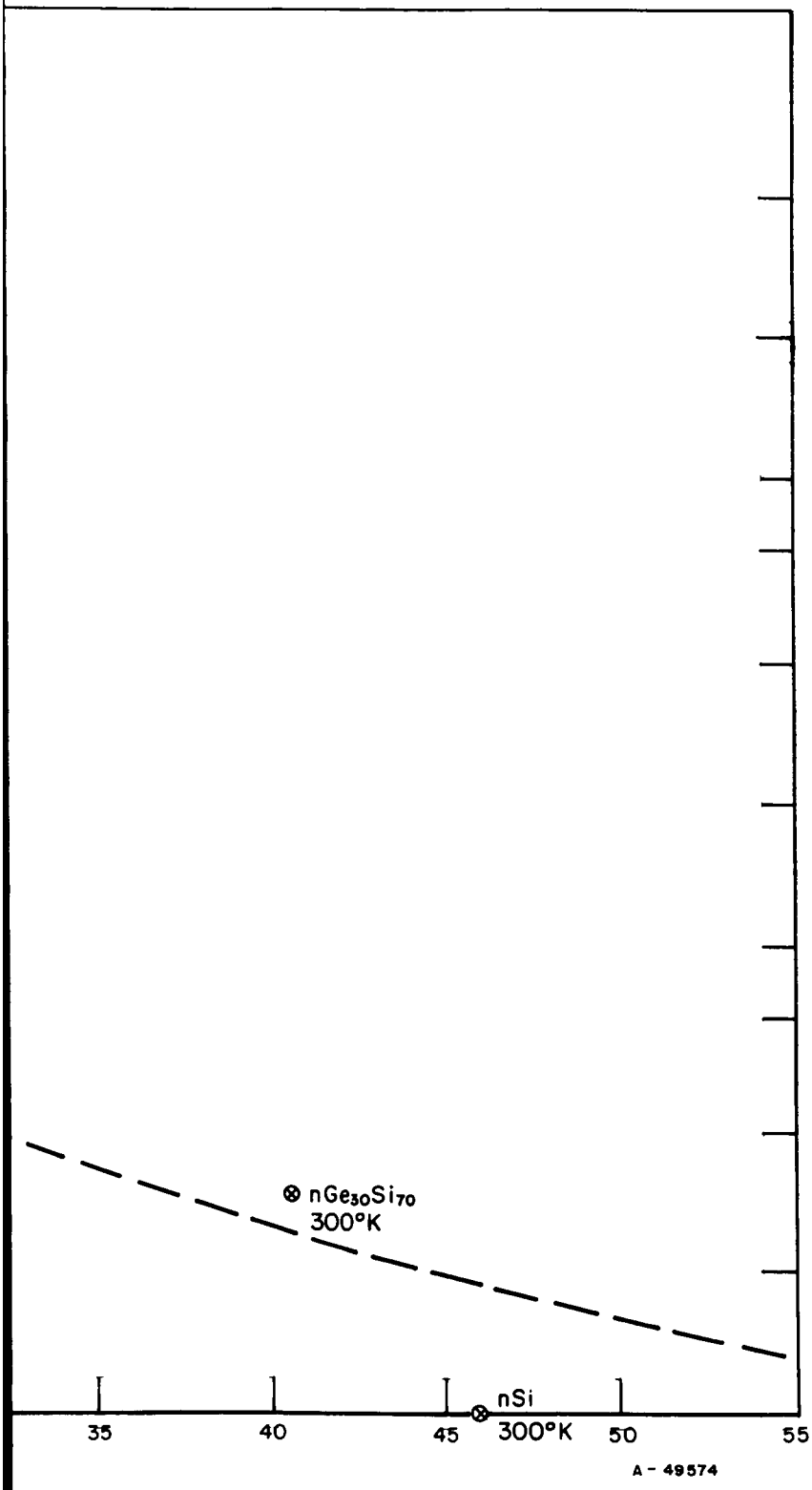
⊗ nGe30Si70
300°K
nSi
300°K
35
40
45
50
55
A - 49574

Values of Z(max)T for both three-band models were determined with the aid of a digital computer program for all combinations of the various parameter values as follows:

$$r = 0,\ 1$$

$$\eta_G = -2,\ 0,\ 2,\ 4,\ 6,\ 8$$

$$\gamma^2 = 1/2,\ 1,\ 2,\ 4$$

$$\beta_e = 8,\ 2,\ 1/2,\ 1/8,\ 1/32$$

$$\eta_{12} = 1,\ 2,\ 3,\ 4,\ 5$$

$$\epsilon = 1.0,\ 0.8,\ 0.6,\ 0.4,\ 0.2 \quad .$$

The values of the optimum Fermi energies at which ZT = Z(max)T were also computed.

Figure 19 shows some representative results of the computations of Z(max)T for n-type material, assuming a single conduction band and a double valence band. The short horizontal lines represent the values of Z(max)T for the two-band case, which corresponds either to $\eta_{12} = 0$ or to $\epsilon = 1.0$. The "fans" of curves above these horizontal lines show the variations of Z(max)T with ϵ and η_{12}.*

Z(max)T for n-type material always increases with increase in η_{12} since removal of the secondary valence band by any amount can only be beneficial. The benefits of increasing η_{12} are relatively greater for smaller ϵ (the higher σ_o valence band being removed) and for greater β_e. The computed values of Z(max)T for the combinations of parameters not shown in Figure 19 show the same patterns of behavior as those that are shown in the figure. The patterns of behavior for the cases of $\gamma^2 \neq 1$, not shown, are similar to those shown for materials with somewhat increased (for $\gamma^2 > 1$) or with somewhat decreased (for $\gamma^2 < 1$) band gaps. In accordance with the approximate relationships given in the Second Quarterly Progress Report, a quantity proportional to $\ln\gamma$ may be added to the actual reduced band gap to obtain the approximately equivalent reduced band gap.

Figure 20 shows some representative Z(max)T computations for n-type material, assuming a double conduction band and a single valence band. The Z(max)T variations are more complex in this case. The value of Z(max)T at first increases with increasing η_{12}, rises to a maximum and then decreases, and eventually approaches asymptotically a value lower than that for $\eta_{12} = 0$. This behavior is more pronounced and covers a wider range of η_{12} values for the smaller band-gap materials and for the smaller values of ϵ. The explanation of this behavior is given below.

Increasing the value of η_{12} corresponds to increasing the energy gap between the secondary conduction band and the valence band. Since the value of Z(max)T for small-band-gap materials is critically limited by the value of the band gap, increasing the gap between even one of the conduction bands and the valence band serves to improve Z(max)T. The degree of this improvement is understandably greater if the σ_o-value of the secondary conduction band, $(1-\epsilon)\sigma_{oe}$, forms a greater percentage of the total σ_{oe}

*The absence of "fans" of curves on some horizontal lines indicates either that Z(max)T is too insensitive to ϵ or η_{12} to be able to plot resolved individual curves on the ordinate scale used, or that there would be a confusing overlap with fans already plotted. The latter would occur for the horizontal lines that are too closely spaced.

value for both conduction bands, corresponding to a smaller value of ϵ. The initial increase of Z(max)T with increasing η_{12} is thus seen to be for the same reason as that for the former case of the single conduction band and double valence band. In the former case the Fermi level is chosen to obtain optimum doping for the single conduction band. In this case, however, the Fermi level must be chosen for the optimum compromise in the carrier concentrations of the two conduction bands. The optimum Fermi level at first rises with increasing η_{12} as would be required to take best advantage of the increased band separation by suitably populating the uppermost band with electrons. However, as η_{12} is still further increased, it becomes increasingly difficult to compromise between the desirability of suitably populating the secondary band and the undesirability of obtaining too high a carrier concentration in the primary band. Eventually this compromise becomes impossible and the best ZT value must correspond to optimum carrier concentration for the primary band alone. This latter limiting Z(max)T value (the asymptotic value mentioned above) is that for a two-band material with the original value of γ^2 (for $\eta_{12}= 0$) reduced to $\epsilon\gamma^2$ (for $\eta_{12} \rightarrow \infty$). It can be seen from the above discussion why the smaller values of ϵ should correspond to the higher maxima but to the lower asymptotic values of Z(max)T as η_{12} is increased. For many of the curves shown in Figure 20, the asymptotic values of Z(max)T are not yet approached for the cases of $\epsilon = 0.6$, 0.4, and 0.2, even for $\eta_{12} = 5$.

The results of sample computations of S and ZT as functions of the Fermi energy for a limited number of values of the parameters of the three-band model are reported in detail in the Third Quarterly Progress Report. These results indicate the absence of any significant qualitative differences in the forms of these functions between the three-band and the two-band models. The existence of only two extrema in S and, consequently, a double maximum in ZT is also predicted by the three-band model. Such differences as do exist in the detailed shapes of the curves and in the positions of their maxima between the two- and the three-band cases represent essentially perturbations of the basic two-band behavior. This raises the possibility of formulating empirical rules for establishing approximately equivalent two-band models of reasonable accuracy for multiband cases. The usual degree of success obtained with two-band models in analyzing the thermoelectric behavior of materials with unknown band structures attests to this possibility. Examination of the results of the extended Z(max)T computations with the three-band model show that rules can be set up for formulating approximately equivalent two-band models over certain ranges of values of the three-band parameters of interest but not over all ranges. These rules are discussed in the Third Quarterly Progress Report.

Possible Material-Selection Criteria

The relationships outlined above between Z(max)T and the pertinent basic material parameters of the one-, two-, and three-band models lead to certain material-selection criteria in terms of these parameters. For example, materials with higher values of both β exp r and $\eta_G + 2.89 \ln \gamma$ would be desired, as previously mentioned. It would be advantageous to be able to translate these requirements based on the electron-energy band model into criteria for preselecting materials for electrical measurements on the basis of chemistry, crystallography, mechanical properties, or other disciplines. An example of a general selection criterion of these latter types is Mooser and Pearson's rules for which chemical compounds should be semiconductors in their crystalline states.[20] The possibilities of establishing such criteria based on crystalline anisotropy and on the degree of ionicity in the chemical bond are discussed below.

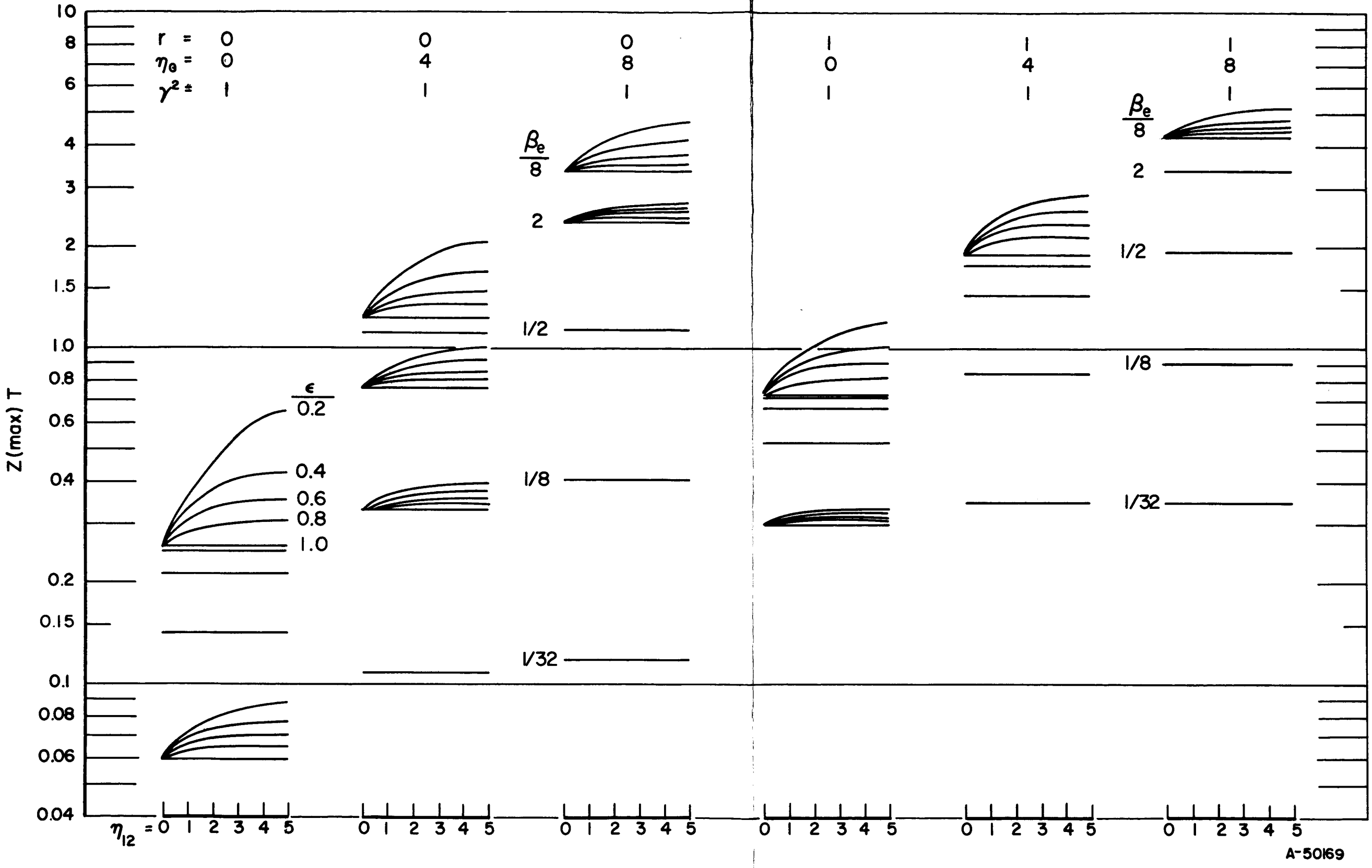

FIGURE 19. FIGURE OF MERIT OF n-TYPE MATERIAL FOR THE THREE-BAND MODEL AS FUNCTION OF REDUCED BAND SEPARATION OF THE ASSUMED TWO VALENCE BANDS

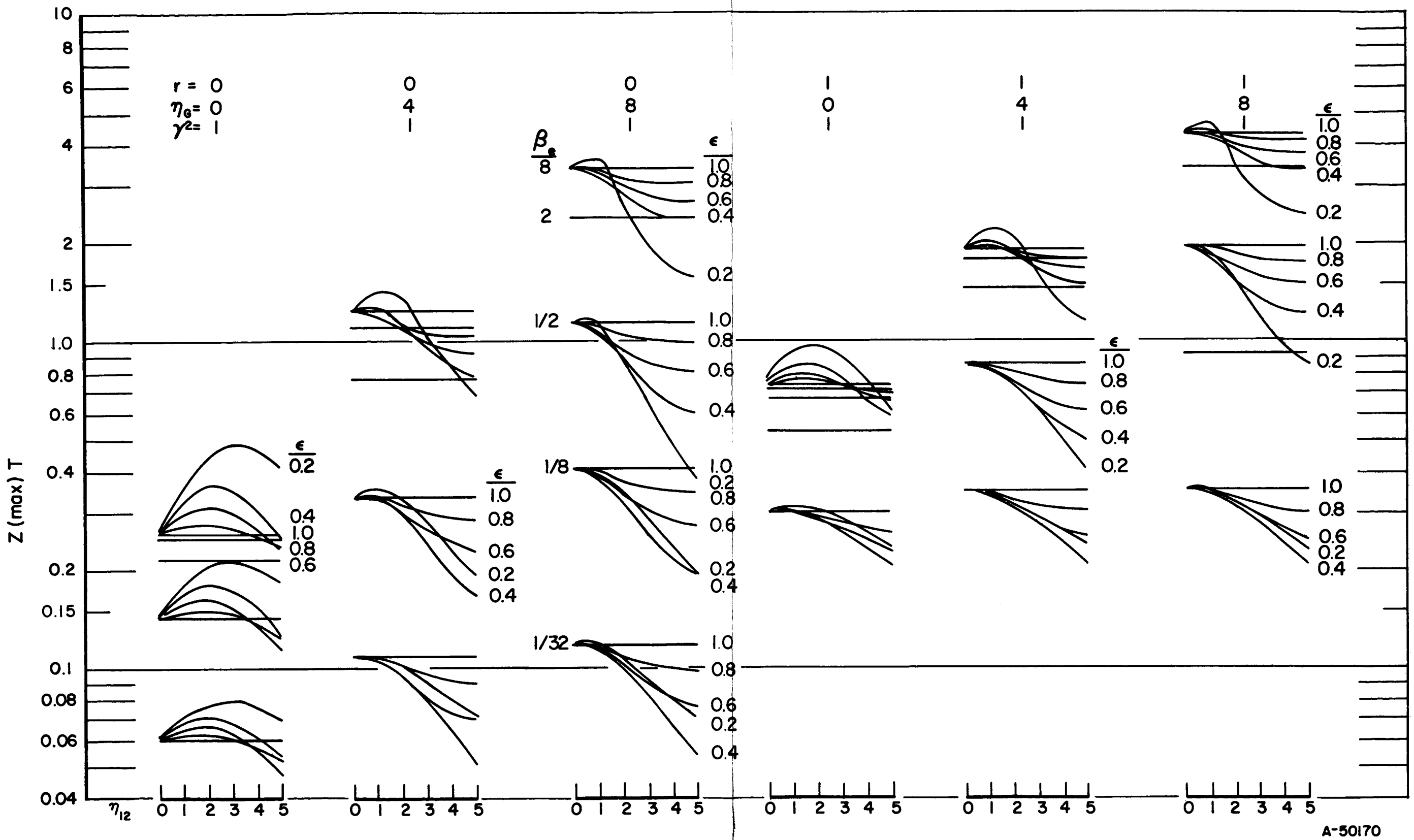

FIGURE 20. FIGURE OF MERIT OF n-TYPE MATERIAL FOR THE THREE-BAND MODEL AS FUNCTION OF REDUCED BAND SEPARATION OF THE ASSUMED TWO CONDUCTION BANDS

Crystalline Anisotropy. For crystals of cubic symmetry, μ_c as given by Equation (3) is reducible to $(1/3)(\mu_1 + \mu_2 + \mu_3)$, regardless of the current direction in the crystal. The quantity σ_o as given by Equation (2) becomes proportional to $N(m_1 m_2 m_3)^{1/2}(m_1^{-1} + m_2^{-1} + m_3^{-1})$ since the density-of-states mass $m_d = (m_1 m_2 m_3)^{1/3}$ and each partial mobility $\mu_i = e\tau/m_i (i = 1, 2, 3)$, assuming the relaxation time τ to be isotropic. It can be readily shown that for a given value of m_d, $m_1^{-1} + m_2^{-1} + m_3^{-1}$ has a minimum value when $m_1 = m_2 = m_3$. Hence, an energy-band structure with a large multiplicity of valleys (because of the factor N) and with a high degree of mass anisotropy per valley is favorable for obtaining larger values of σ_o, and hence of β. If the energy minima do not occur on any of the symmetry axes in the Brillouin zone, it is theoretically possible to have N as high as 48 for a cubic crystal, but values of N greater than about 8 have not been identified for any material.

For crystals of lower symmetry than cubic, it is always possible, in principle, to choose a current direction in which the mobility as given by Equation (3) would be a maximum, thus obtaining a higher value of $m_d^{3/2}\mu_c$ than for the case of cubic symmetry for the same values of m_1, m_2, and m_3 for each energy ellipsoid. The gain in the value of σ_o so obtained would have to be weighed against the possible loss from the reduction in the value of N resulting from the reduced degree of symmetry. For example, consider a crystal of cubic symmetry with N = 4, corresponding to conduction-band energy minima at the boundaries of the Brillouin zone in the (111) directions. Strain of the cube along a (111) direction so as to raise the energy level of the minimum in that direction would result in a crystal of rhombohedral symmetry, with N = 3 in the primary conduction band. It can be shown that the value of σ_o even for the best current orientation must be decreased by removal of the single energy minimum, assuming that the values of m_1, m_2, m_3, and τ are not appreciably affected by the uniaxial strain. Since many crystalline forms are topologically equivalent to distorted cubic structures, considerations analogous to the strained-cube case could be applied; that is, everything else being equal, the generally reduced value of N permitted by the lower order of space symmetry would tend to decrease σ_o. For some cases of multiband conduction, however, distortions of the cubic crystal may tend to reduce the energy difference between two different energy bands of like carriers or increase the energy differences between bands of unlike carriers, thereby tending to increase Z(max)T.

The factor of primary importance thus seems to be the degree of anisotropy per energy ellipsoid and the number of them, not the degree of overall conduction anisotropy of the crystal. Some of the better thermoelectric materials, such as the lead salts and the silicon-germanium alloys, have cubic symmetry. Others are mildly anisotropic, such as Bi_2Te_3 and the Bi-Sb alloys. It will be seen later that the cubic crystals Si and Ge have the highest known values of σ_o for the conduction band, whereas the highly anisotropic pyrolytic graphite crystal happens to have the highest σ_o value for the valence band. No clear-cut advantage seems to be indicated by the σ_o considerations for any particular type of crystal structure.

The question then arises as to how to choose materials whose electronic energy-band structures would be more likely to be characterized by a large multiplicity of equivalent extrema with a high degree of mass anisotropy per extremum. This condition should preferably be characteristic of only one of the energy bands, say the conduction band for n-type material. The other band should have a single extremum of isotropic mass at the center of the Brillouin zone so as to obtain a higher value of $\gamma = (\sigma_{oe}/\sigma_{oh})^{1/2}$, which would be an important consideration if the energy gap is small.

The number of energy extrema in wave number vector ($\vec{k}$) space, their positions, and the values of the effective masses in the three principal directions in the neighborhood of each extremum, $(h^2/4\pi^2)(\partial^2 E/\partial k^2)^{-1}$, depend upon the details of the E versus $\vec{k}$ relationship. This relationship is obtained from the solution of the one-electron Schrödinger equation in the three-dimensional periodic electrostatic potential that an electron "sees" in the crystal lattice. This periodic potential has, of course, the same space-group symmetry as that of the crystal lattice itself. Its value as a function of position in space depends partly on the spatial distributions of the valence electrons, and hence on the types of chemical bonding among the various atoms of the crystal, and partly on the distributions of the nonvalence electrons about the nuclei. The latter is a particularly important factor for the electron-energy band determination because of the large potential gradients in the neighborhoods of these "core" positions, but it has a relatively smaller effect on the chemical bond. The absence of any good general correlation between chemical properties and electron-energy-band structure is thus understandable, although many specific correlations have been found among members of a set of related compounds, such as between the chemical bond energy and the band gap in semiconductors of the diamond or zinc-blende structure.[21] Even in this case, however, the correlation is a good one only among members of the same group, e.g., the III-V compounds, and not across group lines.

Ionicity. Suchet, et al,[22, 23] have discovered a correlation between certain measures of the degree of ionicity of the chemical bond and the electron mobility for the III-V compounds. (Suchet's indicated correlations for the other groups of compounds are questionable.) However, the quantity $\sigma_o e^r$ for optical-mode scattering is independent of μ, since $\mu \propto m^{-3/2}$ according to the perturbation theory of optical-mode lattice-vibration scattering[24], which is the case of interest here. In fact, for predominantly polar optical-mode lattice scattering[2],

$$\sigma_o \approx (8/3\pi)(kT/h)(\epsilon_\infty^{-1} - \epsilon_o^{-1})^{-1} \quad , \tag{4}$$

which is not directly dependent on any of the band-structure variables. In Equation (4), ϵ_o and ϵ_∞ are the low- and high-frequency limiting values of the dielectric constant, respectively.

Although of no value as a thermoelectric rating criterion among a group of materials whose charge-carrier scattering is predominantly by optical-mode lattice vibrations, the possibility that the value of the mobility alone might serve as a rating criterion among a group of materials with mixed optical- and acoustical-mode lattice scattering may be considered, assuming that a higher mobility is a rough indication of a lower relative contribution of optical-mode scattering. However, the best thermoelectric material among such a group may actually correspond to one with a certain finite percentage of optical-mode scattering other than zero. This is because the increase in the effective value of r for an admixture of a small amount of optical-mode scattering (r = 1) to acoustical-mode scattering (r = 0) would initially more than compensate for the decrease of σ_o in the value of the quantity $\sigma_o e^r$. Larger relative amounts of optical-mode scattering would lower σ_o too rapidly, however. Just what proportion of optical-mode scattering would be optimum remains to be investigated. Analogous results have been obtained from an analysis made for an admixture of ionized-impurity scattering (r = 2) and acoustic-mode lattice scattering[1, 25].

For pure acoustic-mode lattice-vibration scattering, the higher the mobility the greater is the value of $\sigma_o e^r$, since $\mu \propto m^{-5/2}$ for this scattering mode. In fact, σ_o is

given by[2]

$$\sigma_o = (e^2h/3\pi^2)C_{11}/m_cE_1^2 \quad , \tag{5}$$

where m_c is the conductivity effective mass, C_{11} is the longitudinal-wave elastic modulus, and E_1 is the deformation potential. It is not evident how the value of μ for pure acoustic-mode scattering could be related to the Suchet ionicity parameters, however.

The relationship between the degree of ionicity of the chemical bond and the value of the lattice thermal conductivity is discussed by M. Rodot[26] and the variation of K_L among members of series of isoelectronic compounds is discussed by A. V. Ioffe[27]. The distinct decrease in the value of K_L with increasing ionicity is another reason why minimum ionicity would not be expected to yield a maximum value of the material parameter β exp r.

For the two-band model, comparison of Figures 16 and 17 indicates a distinct advantage of r = 1 over r = 0, not only because Z(max)T depends approximately on the combination β exp r but also because the low values of η_G have much less of a deleterious effect on Z(max)T for r = 1 than for r = 0. Optical-mode lattice scattering may thus be distinctly advantageous for materials with small band gaps or band overlaps despite the accompanying decrease in β for this scattering mode; this is particularly apropos in the region where Z(max)T is insensitive to the value of β. The relationship between Z(max)T and β, γ, and η_G becomes insensitive to the value of r only in the upper right-hand region of these curves, corresponding to the as-yet-unobtained large values of Z(max)T.

The general conclusion from the above ionicity considerations is that although a very high degree of ionicity of the chemical bond, such as is characteristic of the strongly polar compounds, is definitely deleterious to thermoelectric behavior, maximum values of Z(max)T and $(ZT)_{max}$ are expected to be obtained with materials with some optimum amount of ionicity in their chemical bonds. The degree of ionicity by itself for materials of moderate polarity should thus be a poor indicator of their thermoelectric quality.

Material Studies

The values of the basic material parameters were computed and tabulated for all of the elementary and binary-compound semiconductors and semimetals for which the necessary information on the various constants involved could be found in the literature. These tabulations are given in Tables 6 through 14 of the Second Quarterly Progress Report and in Tables 5 and 6 of the Third Quarterly Progress Report. The tabulations for the various elemental semiconductors and for the III-V compounds are reproduced in this report for convenience in discussion.

These tabulations apparently substantiate the observations on the proposed material-selection criteria discussed above. They should also aid in the search for any significant correlations that might exist between the basic material parameters of the energy-band model and those of other models.

The two-band model of electronic conduction was assumed for the purpose of making these compilations. The rules that were followed for calculating the parameters of the equivalent two-band models for those materials whose electron-energy-band structures are known to consist of a greater multiplicity of allowed energy bands are discussed in the Second Quarterly Progress Report. The ranges of validity of these rules are discussed in the Third Quarterly Progress Report.

The information needed for computing the values of the basic parameters of the two-band model are the numbers of equivalent energy extrema of the conduction and of the valence band, the effective masses and mobilities of the charge carriers in these valleys, the lattice component of the thermal conductivity, the value of the forbidden energy gap between the conduction and valence bands, and the scattering parameters for the charge carriers. It is understandable that room temperature (T = 300°K) would be the only common temperature at which such data would be available for a wide variety of materials. Consequently, only the room-temperature values of the various parameters are computed and tabulated. As pointed out previously, however, the primary interest would usually be in comparing the thermoelectric potentialities of materials at their optimum temperatures, whatever these might be, rather than at a single, fixed temperature. To aid in using Figure 18 to estimate $(ZT)_{max}$ for each material, the temperature dependences of the charge-carrier mobilities are also tabulated, whenever available. The temperature dependences of the energy gaps are ignored as having only a second-order effect on the variation of η_G with temperature for most materials over the usual ranges of temperature of interest. Other neglected factors, such as the effects of nonparabolicity of the band structure on the variation of effective mass and mobility with temperature and carrier concentration and the activation of additional energy bands with increasing temperature, may lead to greater errors in the estimate of $(ZT)_{max}$ than neglect of the temperature dependence of the energy gap.

All entries in the tables are in the commonly employed physical units of $cm^2/volt\ sec$ for μ, $ohm^{-1}\text{-}cm^{-1}$ for σ_o, watts/cm°C for K, and electron volts for E_G. All other quantities are dimensionless, including the effective masses, which are expressed in the conventional manner in terms of their ratios to the free electron mass. The quantity N denotes the number of equivalent band extrema and m_1, m_2, and m_3 are the three principal effective masses for each extremum. For cubic crystals with extrema on the (100) or (111) axes, for which symmetry dictates the equality of the two transverse masses, the designations $m_\perp$ and $m_\parallel$ are employed. The listing of a single mass value does not necessarily imply that the energy band in question has only a single extremum at the center of the Brillouin zone; only a total density-of-states mass value may be known for that particular material. The prefix n before the name of a compound designates that the constants pertinent to the conduction band are listed on that row. The prefix p refers to the valence band, with subscripts, ℓ, h, and so, designating light-hole, heavy-hole, and split-off bands, respectively. At T = 300°K and in terms of the above units, $\sigma_o = 4.00\ N m_d^{3/2}\ \mu$, and $\beta = 2.23 \times 10^{-6}\ \sigma_o/K_L$.

Elemental Semiconductors. Table 6 lists the data and results of the computations for the elemental semiconductors of cubic symmetry (Group IV), with the data for the best known semiconductors, silicon and germanium, forming the only complete set of information in this table. The data for the elemental semiconductors or semimetals of noncubic symmetry are given in Table 7 for pyrolytic graphite and tellurium, Table 8 for bismuth and antimony, and Table 9 for a Bi-Sb alloy.

TABLE 6. BASIC MATERIAL PARAMETERS FOR THE GROUP IV SEMICONDUCTORS

Material	N	$m_{\|\|}$	$m_{\perp}$	$Nm_d^{3/2}$	μ	$\frac{-d \ln \mu}{d \ln T}$	σ_o	$\sigma_o e^r$	K_L	β	γ	E_G, Δ	η_G	References
n-Ge	4	1.588	0.0815	0.410	3,800	1.66	6240	6240	0.61	0.023	2.0	0.66	25.4	28 through 35
p_h	1	0.28		0.148	1,800	2.38	1070					0		
p_l	1	0.044		0.0092	13,500		500					0.28		
p_{so}							1570	1570		0.0057				
n-Si	6	0.90	0.192	1.100	1,450	2.6	6380	6380	1.41	0.010	2.7	1.12	43.0	31,35,36,37
p_h	1	0.49		0.343	500	2.3	690					0		
p_l	1	0.16		0.064	1,500		100					0.044		
p_{so}	1	0.245		0.121	1,000		120							
							910	910		0.0014				
n-C (diamond)		0.25-0.6			900-3900	1.5			5.7			5.6	215	38,39,40
p		0.25-0.6			1200-4800	1.5-2.8								
n-Sn (gray)	4	1.6	0.6	0.304	≈2,000		≈2600					≈0	0	41
	1	0.03		0.0052								≈0		
p	1	0.35		0.207	≈1,000		≈830							
n-β-SiC		0.7			20-100							1.90		42
p		1.2			10-25									

TABLE 7. BASIC MATERIAL PARAMETERS FOR GRAPHITE AND TELLURIUM

Material	N	m_1	m_2	m_3	$Nm_d^{3/2}$	μ	$\frac{-d \ln \mu}{d \ln T}$	σ_o	$\sigma_o e^r$	K_L	βe^r	γ	E_G	η_G	References
n-C-graphite	3	0.031	0.031	0.36	0.0557	12,500	1.2	2780	2780	2-4	~0.0021	0.71	-0.035	-1.35	43,44
p-($\perp$ c-axis)	3	0.066	0.066	0.77	0.1114	16,000	1.2	5560	5560		~0.0041				
n-Te	3	0.374	0.324	0.324	0.594	910		2160		0.023 ($\|\|$ C)			0.34	13	45
p	3	0.123	0.085	0.044	0.0642	570		150							

TABLE 8. BASIC MATERIAL PARAMETERS FOR BISMUTH AND ANTIMONY

Parameter	Bismuth			Antimony			
	n	p	Reference	n	p_l	p_h	Reference
N	3	1		3	3	1	
m_1	0.0062	0.057	(46)	0.068	0.093	≈0.4	(48,49)
m_2	1.30	0.057		0.92	1.14	≈0.4	
m_3	0.0175	0.77		0.050	0.088	0.96	
ϕ	6°			36°	4°		(49)
					27°		(50,51)
$Nm_d^{3/2}$	0.038	0.050		0.164	0.29	≈0.4	
μ_1	32,000	7700	(14)	1500	3600		
μ_2	800	7700		4000	1400		(50,51)
μ_3	19,000	2100		1200	3300		
$\mu_{\parallel}$	19,000	2100		2200	2900		
$\sigma_{o\parallel}$	2,890	420		1450	3400		
$K_{L\parallel}$	0.0087		(47)				
$\beta_{\parallel}$	0.74	0.11					
$\gamma_{\parallel}$	2.6			0.65			
$\mu_{\perp}$	16,600	7700		2500	3000		
$\sigma_{o\perp}$	2,520	1540		1640	3500		
$K_{L\perp}$	0.0170		(47)				
$\beta_{\perp}$	0.33	0.20					
$\gamma_{\perp}$	1.3			0.68			
E_G	-0.10			-0.19			
η_G	-3.8			-7.3			
r	0	0	(47)				

TABLE 9. BASIC MATERIAL PARAMETERS FOR $Bi_{95}Sb_5$

Parameter	$Bi_{95}Sb_5$ n	$Bi_{95}Sb_5$ p	Reference
N	3	1	(52)
m_1	0.0025	0.10	
m_2	0.75	0.10	
m_3	0.0044	0.50	
ϕ	3°		
$Nm_d^{3/2}$	0.0086	0.017	
μ_1			
μ_2			
μ_3			
$\mu_{\parallel}$			
$\sigma_{o\parallel}$			
$K_{L\parallel}$	0.023 (77°K)		(53)
$\beta_{\parallel}$			
$\gamma_{\parallel}$			
$\mu_{\perp}$			
$\sigma_{o\perp}$			
$K_{L\perp}$	0.027 (77°K)		(53)
$\beta_{\perp}$			
$\gamma_{\perp}$			
E_G	0		(53)
η_G	0		
r	0		

The values of σ_o for electrons are about the same for germanium and silicon and represent by far the largest known values of σ_o for any semiconductors. The values of σ_o for the electrons of gray tin, bismuth, and graphite (for conduction in the plane perpendicular to the c-axis) are about the same and represent the second highest σ_o values for electrons for any semiconductors. The σ_o value for the holes in graphite in the high-conductivity plane is almost the same as that for the electrons in silicon or germanium.

The characteristic (β, $\eta_G + 2.89 \ln \gamma$) points for n-Ge and n-Si at room temperature are plotted on Figure 18. The values of β, and consequently of Z(max)T, are low for n-Ge and n-Si at T = 300°K because of the high values of K_L, despite the high values of σ_o. From the positions of these characteristic points about midway between broken-line curves, it can be estimated how the values of Z(max)T for both n-Ge and n-Si would increase with temperature, both reaching $(ZT)_{max}$ values of about 1.0 somewhere near their respective melting points. Actually, since the electron mobilities of germanium and silicon decrease more rapidly than $T^{-1.5}$, the locus of the characteristic points for n-Ge and n-Si as the temperature is raised may well pass near or below the plotted points on Figure 18 for n- and p-Bi_2Te_3 at T = 300°K.

It is more instructive to consider one of the Ge-Si alloys for which high-temperature thermoelectric data are available. The room-temperature characteristic point for the n-$Ge_{30}Si_{70}$ alloy is also shown on Figure 18. The β-value for this point was computed from the information on the Seebeck coefficient, electrical conductivity, and thermal conductivity given in Reference (54). Despite the appreciably lower value of 1200 ohm^{-1}-cm^{-1} for σ_o for this alloy, β is greater than for either 100 percent silicon or germanium because of the much lower value of K_L for the alloy. The value of $\eta_G + 2.89 \ln \gamma$ for the alloy was chosen by using linear interpolation on the energy gap and on the value of γ between silicon and germanium.

The characteristic point for T = 1100°K for the same $Ge_{30}Si_{70}$ alloy is plotted on Figure 18, also based on data in Reference (54). It is seen that β increases at roughly the same rate with temperature as is represented by the broken lines ($\beta \propto T^2$). It is also seen that $(ZT)_{max}$ for this alloy would be just slightly over 1.40, at η_G corresponding to a temperature of about 1700°K, somewhat above the melting point. Measurements are reported in Reference (54) up to 1300°K. The actually measured value of ZT for this alloy at 1100°K is given in Reference (54) as 1.0, whereas the characteristic point in Figure 17 indicates a Z(max)T value of about 1.1. This shows that the particular specimen in question was almost but not quite optimally doped for 1100°K. The extrinsic carrier concentration for this specimen was $1.5 \times 10^{20}/cm^3$; heavy doping is required because of the high values of m_d and T involved.

It is instructive to plot on the same figure the characteristic point for the n$(Bi_2Te_3)_{90}(Bi_2Se_3)_{10}$ alloy at T = 300°K, computed from the data on this material in Reference (3). This latter characteristic point has about the same value of β but a much lower value of $\eta_G + 2.89 \ln \gamma$ than for n-$Ge_{30}Si_{70}$ at T = 1100°K.

There is thus probably nothing particularly unique about the band structure, crystallography, or chemical bonding of Bi_2Te_3 to which its good thermoelectric properties are attributable. It is a valuable material for thermoelectric-cooling applications because its $(ZT)_{max}$ point occurs near room temperature. In n-$Ge_{30}Si_{70}$ with an entirely different structure, bonding, and crystallography we have a material whose thermoelectric properties are superior to those of the Bi_2Te_3 alloy at the optimum temperatures for both materials, at two to three times their respective Debye temperatures.[55] (Also

plotted on Figure 18 is the 82°K characteristic point for $n(Bi_2Te_3)_{90}(Bi_2Se_3)_{10}$ to show that its temperature dependence is "normal".)

Both bismuth and antimony have the same rhombohedral crystal symmetry as Bi_2Te_3. A detailed account of the crystal chemistry and of the band-structure computations for the Group V semimetals is given by Cohen, Falicov, and Golin[56]. This account includes a discussion of the related IV-VI compound semiconductors, PbS, PbSe, PbTe, and SnTe, which have the NaCl cubic structure, and of the semimetal GeTe which has the same rhombohedral structure as bismuth and antimony. The rhombohedral structures of these materials are shown to represent only a slight distortion of the NaCl structure. The (Sn, Ge)Te alloys show a continuous transition from the cubic to the rhombohedral structure and a corresponding transition from semiconducting to semimetallic behavior with increasing concentration of germanium[56].

The conduction band of both bismuth and antimony consists of three equivalent ellipsoids. One of the principal axes of each ellipsoid, labelled Axis 1, is oriented in one of the binary directions. The binary directions are the directions of the twofold axes of rotational symmetry that lie in the basal plane. The (2) and (3) principal axes are tilted somewhat away from the bisectrix and trigonal directions, respectively, by about 6° toward the bisectrix direction for the (3) axis of bismuth and by about 36° in the opposite sense for antimony. The trigonal direction is the direction of the threefold axis of symmetry (the c-axis) perpendicular to the basal plane. The three bisectrix directions lie in the basal plane and are perpendicular to the three respective binary axes.

If μ_1, μ_2, and μ_3 are the partial mobilities corresponding to charge transport along the 1, 2, and 3 axes, respectively, and ϕ is the angle of tilt, the electron mobility along the trigonal axis is given by

$$\mu_e\| = \mu_2 \sin^2\phi + \mu_3 \cos^2\phi \quad . \tag{6}$$

The electron mobility is isotropic in the basal plane ($\perp$ to the c-axis) and is given by

$$\mu_e\perp = (\mu_1/2) + (\mu_2/2)\cos^2\phi + \mu_3 \sin^2\phi \quad . \tag{7}$$

It is seen that if ϕ is small, then for all practical purposes, $\mu_e\| = \mu_3$ and $\mu_e\perp = (\mu_1 + \mu_2)/2$. Equations (6) and (7), which apply only in zero or weak magnetic fields, were employed to obtain the values of $\sigma_o\|$ and $\sigma_o\perp$ for electrons in Table 8, with the aid of Equation (2).

The valence band of bismuth is a spheroid with its axis of revolution about the trigonal axis. The valence band of antimony, however, is of the three-valley type, with the constant-energy surfaces almost spheroidal and tilted about 36° from the trigonal axis. Presumably, as discussed previously for the conduction bands of germanium and silicon, both bismuth and antimony have both types of valence bands, the primary valence bands being those mentioned above. Consequently, for some range of composition of the Bi-Sb alloys in the neighborhood of the crossover point in the energy levels of the two valence bands, the three-band model would be more appropriate for the analysis of the thermoelectric behavior of these alloys. Experimental evidence for the existence of a second valence band in bismuth is still inconclusive.[48, 57] There is considerable evidence for the existence of a double valence band in antimony,[48, 58] however; in particular, inconsistencies are obtained in attempting to analyze room-temperature galvanomagnetic data for pure and doped antimony on the basis of the two-band model.[48, 51] It

has also not been found possible to account for both the magnetic-field and temperature variations of various galvanomagnetic effects in the $Bi_{94.5}Sb_{5.5}$ alloy by use of the two-band model alone[59].

The partial-mobility values listed for antimony in Table 8 were obtained by assuming the two-band model, so that the values of σ_{oe} and σ_{oh}, both parallel and perpendicular to the c-axis, obtained by combining these mobility values with the listed effective masses, may be questionable. Even for the case of bismuth, the best known of these materials, sizable variations may be found in the literature among the effective-mass values obtained by various methods; see, for example, Table 1 of Reference (60).

It may be seen in Table 8 that the values of both σ_{oe} and σ_{oh} for both bismuth and antimony are unusually high, with the sole exception of $\sigma_{oh}\| = 420$ ohm^{-1}-cm^{-1} for bismuth. With the exception of σ_{oh} for bismuth, all values of σ_{oe} and σ_{oh} are only moderately anisotropic.

For the Bi-Sb alloys, Jain[61] ascertained that the energy gap is positive for antimony concentrations between 5 and 40 atomic percent, reaching a maximum of 0.014 ev at about 12 percent. It appears that there is a change from a bismuth-like to an antimony-like valence band structure when the antimony concentration exceeds 12 percent[62]. Brown and Silverman[60] present some evidence that the $Bi_{85}Sb_{15}$ alloy may have a band gap as high as 0.024 ev.

Despite a considerable amount of effort in the last few years in measuring and analyzing the various properties of Bi-Sb alloys, there is little information available in the literature to permit anywhere near a complete compilation of the values of the various basic material parameters for the different Bi-Sb alloys, as listed for pure bismuth in Table 8. Cyclotron-resonance measurements have been reported for the components of the effective-mass tensors for the electrons and for the holes in $Bi_{95}Sb_5$; these are listed in Table 9, combined with some information on the lattice thermal conductivity and the band gap.

The meager and imprecise knowledge regarding the basic material parameters of the Bi-Sb alloys precludes making any meaningful analysis at present to determine the value of Z(max)T at a given temperature as a function of alloy composition, or of $(ZT)_{max}$, the best value of Z(max)T as a function of temperature, for a given alloy. The picture will become clearer, of course, as more data are accumulated. Of particular value in this respect would be information on the variations of the Seebeck coefficient, the electrical conductivity, and the thermal conductivity of given alloys as the impurity doping is varied.

For conduction parallel to the c-axis in bismuth at room temperature, we have $\beta_e = 0.71$, $\gamma = 2.6$, and $\eta_G = -0.38$. The predicted value of Z(max)T for n-type bismuth at room temperature (at optimum doping) is just about 0.50, in accordance with either Figure 16 or 18, assuming the equivalent two-band model to apply at room temperature. The value of Z(max)T would approach about 0.58 as $\beta_e \to \infty$, in accordance with Figure 12 of the Second Quarterly Progress Report. The main purpose of alloying bismuth and antimony for possible thermoelectric applications near room temperature, unlike the purpose of alloying for most other materials, is thus not to increase β_e but to increase the energy gap. For $\eta_G = 0$ rather than -0.38 and for the same values of β_e and γ as for bismuth, the predicted value of Z(max)T would be about 0.60. Any improvement in Z(max)T that may occur from increasing β by alloying would be more noticeable at the lower temperatures, however, where β is smaller and Z(max)T is more sensitive to the value of β.

Smith and Wolfe[63] obtained an experimental value of about $1.3 \times 10^{-3}/°K$ for the figure of merit of pure bismuth along the c-axis at room temperature, corresponding to a ZT value of about 0.39. Their 5 percent antimony alloy had the highest ZT (= 0.54) at room temperature. Their measured value of Z for Bi at 80°K was also $1.3 \times 10^{-3}/°K$, resulting in ZT = 0.10 at this temperature. However, they obtained $Z \approx 5.0 \times 10^{-3}/°K$ at 80°K for about the 3 percent to about the 15 percent alloy, corresponding to $ZT \approx 0.4$ at this temperature. Although it is not known how close their specimens are to optimum doping, the qualitative agreement is to be noted between these experimental results and the behaviors predicted in the previous paragraph.

The III-V Compound Semiconductors. Table 10 lists the data and computations of β exp r, γ, and η_G for the III-V compounds. The value of r = 1 has been chosen for computing $\sigma_o e^r$ and $\beta_e{}^r$ since, as pointed out by Ehrenreich,[64] the dominant scattering mechanism for electrons in the III-V compounds at room temperature is by the optical-mode lattice vibrations. This occurs despite the modest degrees of ionicity in these compounds because of the very small values of the electron effective masses. The value r = 1 was chosen arbitrarily for the holes as well as for the electrons for all of the III-V compounds. Although various degrees of mixed scattering would probably give a better representation, the Z(max)T theory for mixed scattering has not yet been developed. It is to be noted that if σ_o exp r is computed from resistivity and Seebeck-coefficient data on extrinsic III-V compounds, values intermediate between those listed in Table 10 for σ_o and for σ_o exp r are obtained.

It is noteworthy that although the electron mobilities for the various III-V compounds range in value over almost three orders of magnitude, the values of σ_o vary over a range of only about 2 to 1 (exclusive of the abnormally low value of σ_o for nGaSb). Despite the much higher electron mobilities of the III-V compounds (excluding GaP and AlSb whose lowest lying conduction band minima consist of three 100 valleys), the values of σ_o for the III-V compounds are an order of magnitude lower than those for silicon and germanium. The primary conduction bands of the III-V compounds, with the above exceptions, are spherical, with single minima at k = 0.

It is to be noted that GaAs has the highest value of σ_o of the n-type III-V compounds at room temperature. InSb, with an order of magnitude higher mobility than that of GaAs, is only a close second in its σ_o value. Hence, even ranking the thermoelectric qualities of the III-V compounds among themselves in accordance with mobility is seen to be of no significance.

TABLE 10. BASIC MATERIAL PARAMETERS FOR THE III-V COMPOUNDS

Material	N	m	$m^{3/2}$	μ	$\frac{-d \ln \mu}{d \ln T}$	σ_o	$r = 1$ $\sigma_o e^r$	K_L	$\beta_e{}^r$	γ	E_G	η_G	References
n-InSb	1	0.014	0.00166	78,000	1.68	520	1420	0.17	0.019	1.58	0.17	6.5	35,65,66, 67,68
p_h	1	0.40	0.0692	750	2.1	210	570		0.0075				
p_l	1	0.02											
n-InAs	1	0.022	0.00326	33,000	1.5	430	1170	0.27	0.0096	1.69	0.36	14	
p_h	1	0.41	0.081	460	>2	150	410		0.0034				
p_l	1	0.025											
n-InP	1	0.067	0.0174	4,600	2	320	870	0.67	0.0029	1.88	1.29	50	
p_h	1	0.4	0.15	150	2.4	90	245		0.00081				
p_l	1	0.07											
n-GaSb	1	0.047	0.0102	Low 4,000	1.5	Low 165	Low 450	0.38		0.63-?	0.67	26	
p_h	1	0.23	0.073	1,400	1.5	410	1120						
p_l	1	0.05-?											
n-GaAs	1	0.068	0.0177	8,800	1	620	1690	0.46	0.0082	1.26	1.35	52	
p_h	1	0.5	0.247	400	2.1	390	1060		0.0051				
p_l	1	0.07-?											
n_h-GaP	3	0.35	0.206	300		250	680	~1.09	~0.0014	1.31			
n_l	1	0.12									2.25	87	
p_h	1	0.4	0.214	170		145	395		0.00081				
p_l	1	0.12-?											
n_h-AlSb	3	0.39	0.243	200-450		~200	540	0.46	0.0026	0.71	1.62	62	
n_l	1	0.09											
p	1	0.4	0.177	200-450		~390	1060		0.0051				

REFERENCES

(1) Simon, R., "Maximum Figure of Merit of Thermoelectric Materials", Adv. Energy Conv., 1, 81 (1961).

(2) Simon, R., J. Appl. Phys., 33, 1830 (1962).

(3) Bate, R. T., Technical Report No. 3 on "Thermoelectric Properties of Bi_2Te_3-Bi_2Se_3 Alloys", to ONR (1960), Contract No. 3316(00) NR 017-434.

(4) Airapetyants, S. V., Sov. Phys.-Tech. Phys., 2, 478 (1957).

(5) Airapetyants, S. V., and Breslev, M. S., Sov. Phys.-Tech. Phys., 3, 1935 (1958).

(6) Beer, A. C., and Bate, R. T., "Effect of Various Impurities on Lattice Thermal Conductivity of Bi_2Te_3", Final Report from Battelle Memorial Institute to Office of Naval Research, Contract No. NONR-2316(00), April 30, 1960.

(7) Cosgrove, G. J., et al, J. Appl. Phys., 32, 621 (1961).

(8) Wolfe, R., et al, J. Appl. Phys., 31, 1959 (1960).

(9) Armstrong, R. W., Faust, J. W., Jr., and Tiller, W. A., J. Appl. Phys., 31, 1954 (1960).

(10) Brown, D. M., and Heumann, F. K., J. Appl. Phys., 35, 1947 (1964).

(11) Kooi, C. F., et al, Lockheed Aircraft Corporation, Interim Engineering Report No. 3, Contract No. AF 33(616)-8490, March, 1962.

(12) Simon, R., Adv. Energy Conv., 4, 237 (1964).

(13) Keyes, R. W., Solid State Phys., 11, 149 (1960).

(14) Abeles, B., and Meiboom, S., Phys. Rev., 101, 544 (1956).

(15) Chasmar, R. P., and Stratton, R. J., J. Electron. Control, 7, 52 (1959).

(16) Simon, R., Adv. Energy Conv., 3, 515 (1963).

(17) Ilisavskii, Yu. V., Thermoelectric Properties of Semiconductors, V. A. Kutasov, ed., p 10, translated by Consultants Bureau, N. Y. (1964).

(18) Long, D., J. Appl. Phys., 33, 1682 (1962).

(19) Beer, A. C., Galvanomagnetic Effects in Semiconductors, p 237, Academic Press, N. Y. (1963).

(20) Mooser, E., and Pearson, W. B., Phys. Rev., 101, 492 and 1608 (1956).

(21) Manca, P., J. Phys. Chem. Solids, 20, 268 (1961).

(22) Suchet, J. P., J. Phys. Chem. Solids, 21, 156 (1961).

(23) Suchet, J. P., Rodot, H., Leroux-Hugon, P., and Rodot, M., Adv. Energy Conv., 3, 569 (1963).

(24) Fröhlich, H., and Mott, N. F., Proc. Roy. Soc. (London), A171, 496 (1939).

(25) Ure, R. W., J. Appl. Phys., 30, 1922 (1959).

(26) Rodot, M., Rev. Gen. Thermique, 3, 1541 (1964).

(27) Ioffe, A. V., Soviet Phys.-Solid State, 5, 2466 (1963), [Translation Journal].

(28) Levinger, B., and Frankl, D., J. Phys. Chem. Solids, 20, 281 (1960).

(29) Price, M. B., Phys. Rev., 92, 681 (1953), and 93, 1204 (1954).

(30) McCarthy, K. A., and Ballard, S. S., Phys. Rev., 99, 1104 (1955).

(31) Dexter, R. N., Zeiger, H. J., and Lax, B., Phys. Rev., 104, 637 (1956).

(32) Dresselhaus, G., Kip, A. F., and Kittel, C., Phys. Rev., 95, 568 (1954), and 98, 368 (1955).

(33) Willardson, R. K., Harman, T. C., and Beer, A. C., Phys. Rev., 96, 1512 (1954).

(34) Macfarlane, G. E., McLean, T. P., Quan, J. E., and Roberts, V., Phys. Rev., 108, 1377 (1957), and 111, 1245 (1958).

(35) Stegmeier, E. F., and Kudman, I., Phys. Rev., 132, 508 (1963).

(36) Rauch, C. J., Stickler, J. J., Zeiger, H. J., and Heller, G. S., Phys. Rev. Letters, 4, 64 (1960).

(37) Morin, F. J., and Maita, J. P., Phys. Rev., 96, 28 (1954).

(38) Robertson, R., Fox, J. J., and Martin, A. E., Phil. Trans., A232, 463 (1934).

(39) Redfield, A. G., Phys. Rev., 94, 526 (1954).

(40) Mitchell, E.J.W., J. Phys. Chem. Solids, 8, 444 (1958).

(41) Groves, S. H., ONR Technical Report No. HP-10 (Dec. 1963) NR-017-308, Contract No. Nonr-1866(10).

(42) O'Connor, J. R., and Smiltens, J., Ed., SiC, A High Temperature Semiconductor, Pergamon Press (1960).

(43) Soule, D. E., and McClure, J. W., J. Phys. Chem. Solids, 8, 29 (1959).

(44) Klein, C. A., and Holland, M. G., Phys. Rev., 136, A575 (1964).

(45) Benoit de la Guillaume, C., et al, Selected Constants Relative to Semiconductors, Ed. by P. Aigrain and M. Balkanski, Pergamon Press (1961).

(46) Smith, G. E., Hebel, L. C., and Buchsbaum, S. J., Phys. Rev., 129 154 (1963).

(47) Gallo, C. F., Chadrasekhar, B. S., and Sutter, P. H., J. Appl. Phys., 34, 144 (1963).

(48) Hall, J. J., and Koenig, S. H., IBM J. Res. Develop., 8, 241 (1964).

(49) Datar, W. R., and Vanderkooy, J., IBM J. Res. Develop. 8, 247 (1964).

(50) Freedman, S. J., and Juretschke, H. J., Phys. Rev., 124, 1379 (1961).

(51) Epstein, S., and Juretschke, H. J., Phys. Rev., 129, 1148 (1963).

(52) Smith, G. E., Phys. Rev. Letters, 9, 487 (1962).

(53) Hawkins, S. R., Cuff, K. F., and Harshman, J. H., Bull. Am. Phys. Soc., 7, 494 (1962).

(54) Dismukes, J. P., Ekstrom, L., Steigmeier, E. F., Kudman, I., and Beers, D. S., J. Appl. Phys., 35, 2899 (1964).

(55) Gul'tyaev, P. V., and Petrov, A. V., Sov. Phys. - Solid State, 1, 330 (1959).

(56) Cohen, M. H., Falicov, L. M., and Golin, S., IBM J. Res. Develop., 8, 215 (1964), Proceedings of the Conference on the Physics of Semimetals, Columbia University, January 21, 1964.

(57) Jain, A. L., and Koenig, S. H., Phys. Rev., 127, 442 (1962).

(58) Nanney, C., Phys. Rev., 129, 109 (1963).

(59) Hashimoto, K., and Beer, A. C., unpublished.

(60) Brown, D. M., and Silverman, S. J., Phys. Rev., 136, A290 (1964).

(61) Jain, A. L., Phys. Rev., 114, 1518 (1959).

(62) Goldsmid, H. J., Thermoelectric Refrigeration, Plenum Press, N. Y., p 121 (1964).

(63) Smith, G. E., and Wolfe, R., J. Appl. Phys., 33, 841 (1962).

(64) Ehrenreich, H., J. Appl. Phys., 32, 2155 (1961).

(65) Steigmeier, E. F., and Kudman, I., Phys. Rev., 132, 508 (1963).

(66) Hilsum, C., and Rose-Innes, A. C., Semiconducting III-V Compounds, Pergamon Press (1961).

(67) Hilsum, C., "Band Structure, Effective Charge and Scattering Mechanisms in III-V Compounds", paper presented at Paris Conference on Semiconductors (1964).

(68) Bube, R. H., Photoconductivity of Solids, John Wiley (1960).

* * * * *

Data on which this report is based are recorded in Battelle Laboratory Record Books Nos. 21561, pp 1-100; 21590, pp 1-77; and 22086, p 41.

EPS:LKM:BGK:RS:EHL/eh

Distribution List

Mr. H. F. Powell
Director of Appliance Engineering and Research
Kelvinator Division
American Motors Corporation
14250 Plymouth Road
Detroit 32, Michigan

Dr. L. V. Sloma
Associate Director, Physics and Electronics
Roy C. Ingersoll Research Center
Borg-Warner Corporation
Des Plaines, Illinois

Mr. Donald J. Henry
Head, Metallurgical Engineering Department
Research Laboratories
General Motors Corporation
Box 188, North End Station
Detroit 2, Michigan

Mr. A. T. Bassett
Frigidaire Division
General Motors Corporation
Dayton 1, Ohio

Dr. Kermit F. Cuff
Department 52-40
Electronic Sciences Laboratory
Lockheed Missiles and Space Company
Palo Alto, California 94301